1

Earthquake Characteristics

1.1 Causes of Earthquakes

1.1.1 Plate Tectonics Theory

An earthquake is manifested as ground shaking caused by the sudden release of energy in the Earth's crust. This energy may originate from different sources, such as dislocations of the crust, volcanic eruptions or even by man-made explosions or the collapse of underground cavities, such as mines or karsts. Thus, while earthquakes are defined as natural disturbances, different types of earthquake exist: fault rupture-induced, volcanic, mining-induced and large reservoir-induced. Richter (1958) has provided a list of major earth disturbances recorded by seismographs as shown in Figure 1.1. Tectonic earthquakes are of particular interest to the structural engineers, and further discussion will therefore focus on the latter type of ground disturbance.

Earthquake occurrence may be explained by the theory of large-scale tectonic processes, referred to as 'plate tectonics'. The theory of plate tectonics derives from the theory of continental drift and sea-floor spreading. Understanding the relationship between geophysics, the geology of a particular region and seismic activity began only at the end of the nineteenth century (Udias, 1999). Earthquakes are now recognised to be the symptoms of active tectonic movements (Scholz, 1990). This is confirmed by the observation that intense seismic activity occurs predominantly on known plate boundaries as shown in Figure 1.2.

Plates are large and stable rigid rock slabs with a thickness of about 100 km forming the crust or lithosphere and part of the upper mantle of the Earth. The crust is the outer rock layer with an internal complex geological structure and a non-uniform thickness of 25–60 km under continents and 4–6 km under oceans. The mantle is the portion of the Earth's interior below the crust, extending from a depth of about 30 km to about 2900 km; it consists of dense silicate rocks. The lithosphere moves differentially on the underlying asthenosphere, which

Fundamentals of Earthquake Engineering: From Source to Fragility, Second Edition. Amr S. Elnashai and Luigi Di Sarno.

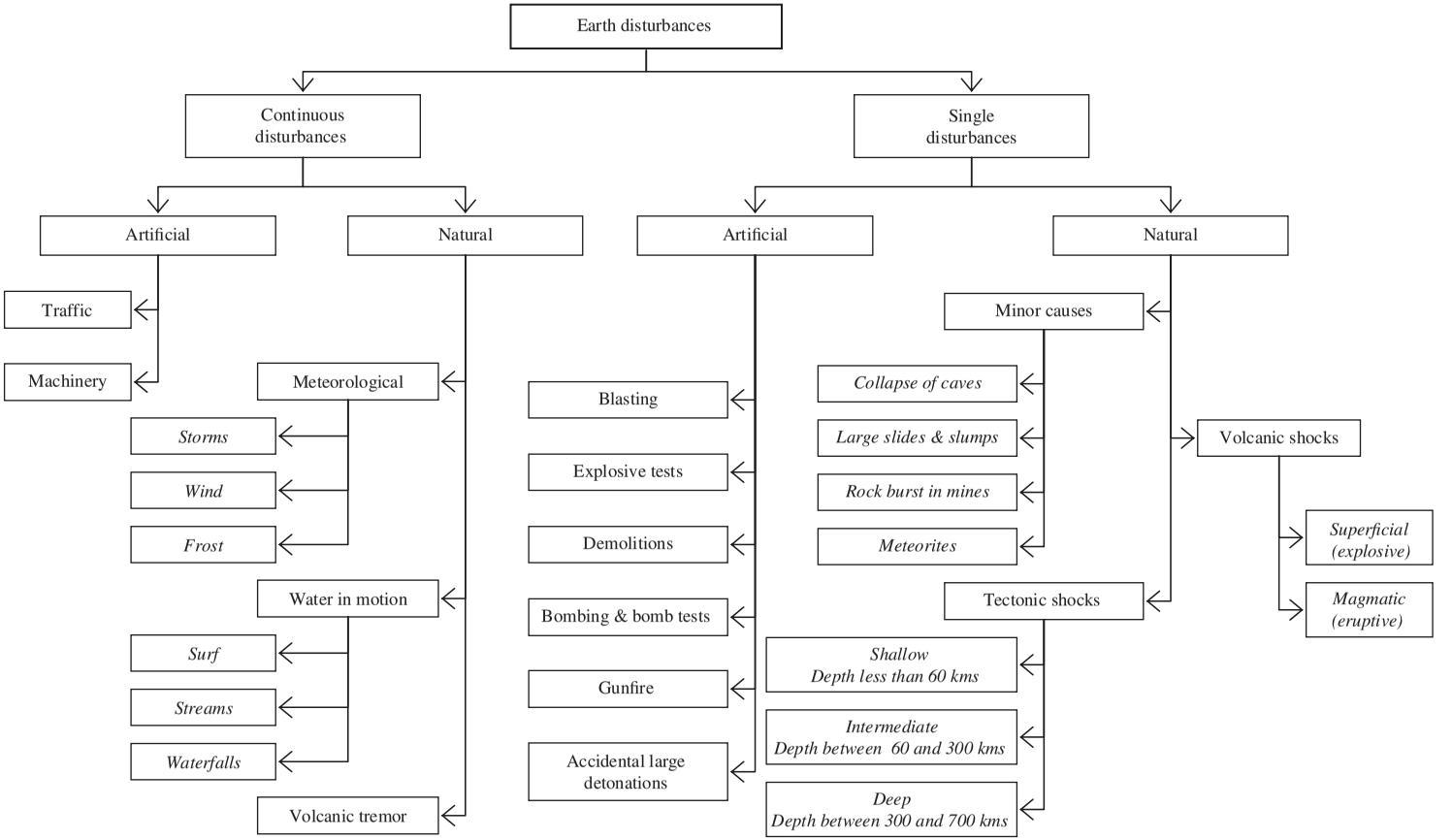

Figure 1.1 Earth disturbances recorded by seismographs.

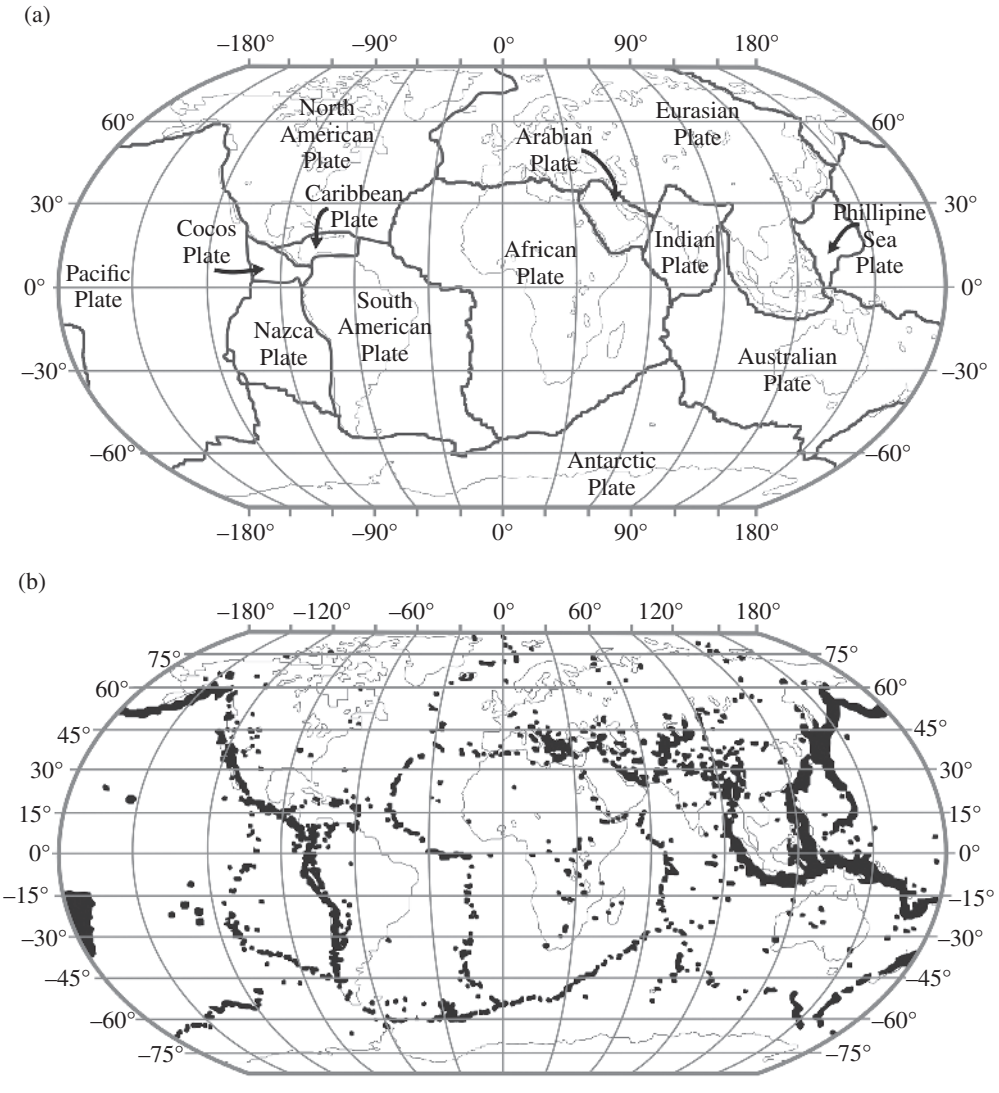

Figure 1.2 Tectonic plates (a) and worldwide earthquake distribution (b). (Adapted from Saint Louis University, Earthquake Center, USA.)

is a softer warmer layer around 400 km thick at a depth of about 50 km in the upper mantle. It is characterised by plastic or viscous flow. The horizontal movement of the lithosphere is caused by convection currents in the mantle; the velocity of the movement is about 1–10 cm/year. Current plate movement can be tracked directly by means of reliable space-based geodetic measurements, such as very long baseline interferometry, satellite laser ranging and global positioning systems.

Large tectonic forces take place at the plate edges due to the relative movement of the lithosphere–asthenosphere complex. These forces instigate physical and chemical changes

and affect the geology of the adjoining plates. However, only the lithosphere has the strength and the brittle behaviour to fracture, thus causing an earthquake.

According to the theory of continental drift, the lithosphere is divided into 15 rigid plates, including continental and oceanic crusts. The plate boundaries, where earthquakes frequently occur, are also called 'seismic belts' (Kanai, 1983). The Circum-Pacific and Eurasian (or Alpine) belts are the most seismically active. The former connects New Zealand, New Guinea, the Philippines, Japan, the Aleutians, the west coast of North America and the west coast of South America. The 1994 Northridge (California) and the 1995 Kobe (Japan) earthquakes occurred along the Circum-Pacific belt. The Eurasian belt links the northern part of the Mediterranean Sea, Central Asia, the southern part of the Himalayas and Indonesia. The Indian Ocean earthquake of 26 December 2004 and the Kashmir earthquake of 8 October 2005 were generated by the active Eurasian belt.

The principal types of plate boundaries can be grouped as follows (Figure 1.3):

(i) *Divergent or rift zones:* plates separate themselves from one another and either an effusion of magma occurs or the lithosphere diverges from the interior of the Earth. Rifts are distinct from mid-ocean ridges, where new oceanic crust and lithosphere is created by sea-floor spreading. Conversely, in rifts no crust or lithosphere is produced. If rifting continues, eventually a mid-ocean ridge may form, marking a divergent boundary between two tectonic plates. The Mid-Atlantic ridge is an example of a divergent plate boundary. An example of rift can be found in the middle of the Gulf of Corinth, in Greece. However, the Earth's surface area does not change with time and hence the creation of new lithosphere is balanced by the destruction at another location of an equivalent amount of rock crust, as described below.

(ii) *Convergent or subduction zones:* adjacent plates converge and collide. A subduction process carries the slab-like plate, known as the 'under-thrusting plate', into a dipping zone, also referred to as the 'Wadati–Benioff zone', as far downward as 650–700 km into the Earth's interior. Two types of convergent zones exist: oceanic and continental

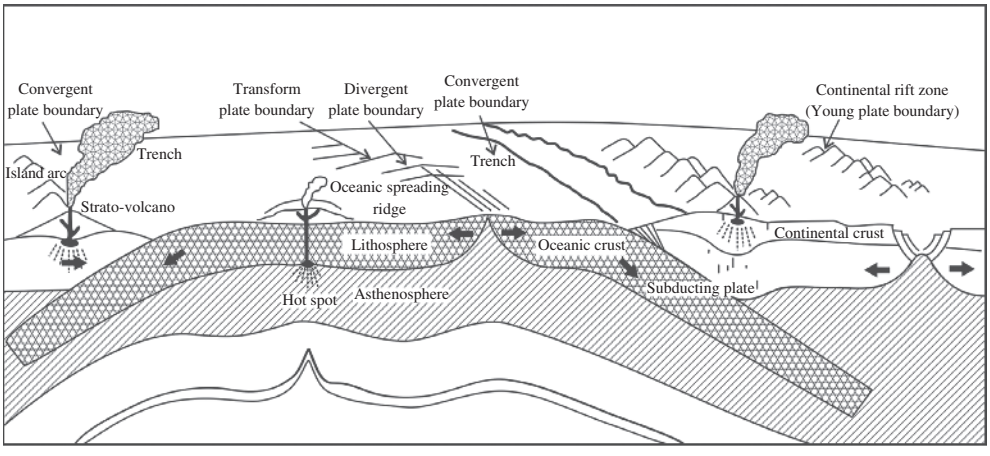

Figure 1.3 Cross-section of the Earth with the main type plate boundaries. (Adapted from USGS.)

lithosphere convergent boundaries. The first type occurs when two plates consisting of oceanic lithosphere collide. Oceanic rock is mafic, and heavy compared to continental rock, therefore it sinks easily and is destroyed in a subduction zone. The second type of convergent boundary occurs when both grinding plates consist of continental lithosphere. Continents are composed of lightweight rock and hence do not subduct. However, in this case the seismicity is extended over a wider area. The Circum-Pacific and Eurasian belts are examples of oceanic and continental lithosphere convergent boundaries, respectively.

(iii) *Transform zones or transcurrent horizontal slip:* two plates glide past one another but without creating new lithosphere or subducting old lithosphere. Transform faults can be found either in continental or oceanic lithosphere. They can offset mid-ocean ridges, subduction zones or both. Boundaries of transcurrent horizontal slip can connect either divergent and convergent zones or two convergent zones. The San Andreas Fault in California is an example of a transform boundary connecting two spreading ridges, namely the North America and Pacific plates in the Gulf of California to the south and the Gorda Ridge in the north.

High straining and fracturing of the crustal rocks is caused by the process of subduction. Surface brittle ruptures are produced along with frictional slip within the cracks. Strain is relieved and seismic energy in the form of an earthquake is released.

Earthquakes normally occur at a depth of several tens of kilometres, with some occasionally occurring at a depth of several hundred kilometres. Divergent plate boundaries form narrow bands of shallow earthquakes at mid-oceanic ridges and can be moderate in magnitude. Shallow and intermediate earthquakes occur at convergent zones in bands of hundreds of kilometres wide. Continental convergence earthquakes can be very large. For example, the 1897 Assam (India) earthquake caused extensive damage and surface disruption, necessitating the upgrade of the intensity model scale used for measuring earthquakes (Richter, 1958). Deep earthquakes, for example between 300 and 700 km in depth, are generally located in subduction zones over regions which can extend for more than 1,000 km. These earthquakes become deeper as the distance from the oceanic trench increases as shown in Figure 1.4. However, the seismic Wadati–Benioff zones are limited to the upper part of the subduction zones, that is about 700 km deep. Beyond this depth, either the plates are absorbed into the mantle or their properties are altered and the release of seismic energy is inhibited. Shallow earthquakes with large magnitude can occur along transform faults. For example, Guatemala City was almost destroyed during the devastating 1976 earthquake which occurred on the Motagua fault. The latter constitutes the transform boundary between two subduction zones, located respectively off the Pacific Coast of Central America and the Leeward and Windward Islands in the Atlantic Ocean.

Plate tectonic theory provides a simple and general geological explanation for plate boundary or inter-plate earthquakes, which contribute 95% of worldwide seismic energy release. It is, however, to be noted that earthquakes are not confined to plate boundaries. Local small magnitude intra-plate earthquakes, which may occur virtually anywhere, can cause considerable damage. Several examples of such events exist and the devastating effects are well documented (e.g. Scholz, 1990; Bolt, 1999, among others). The Newcastle (Australia) earthquake of 28 December 1989 caused about 30 deaths and $750 million in economic loss. The Dahshour (Egypt) earthquake of 12 October 1992 caused damage

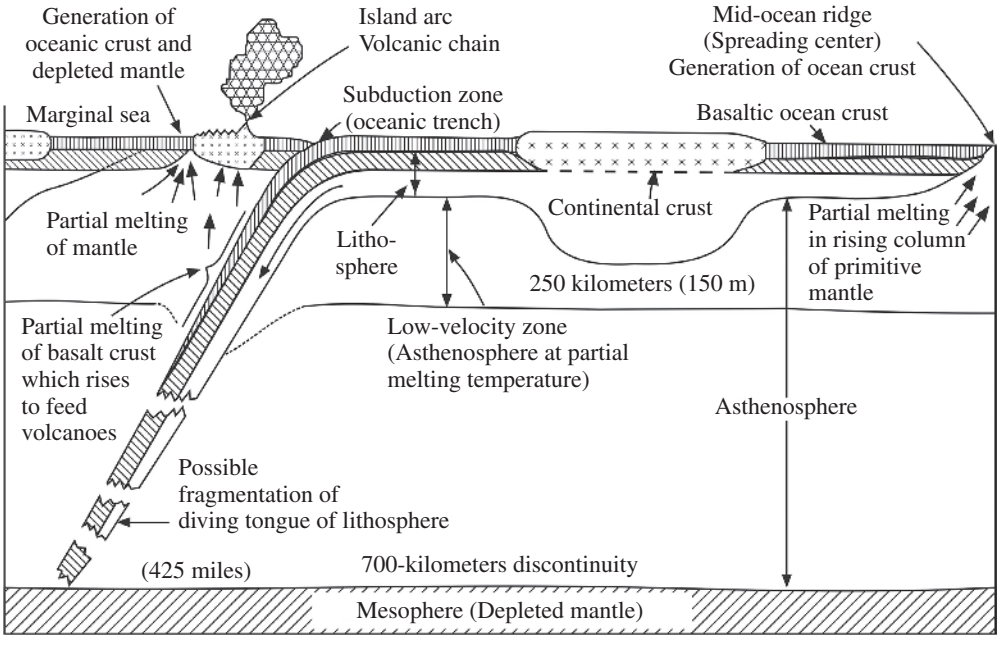

Figure 1.4 Tectonic mechanisms at plate boundaries. (After Dewey, 1972.)

Table 1.1 Classification of tectonic earthquakes.

Earthquake (type)	Slip rate (v) (mm/year)	Recurrence time (year)
Inter-plate	$v > 10$	~100
Intra-plate (*plate boundary related*)	$0.1 \le v \le 10$	10^2–10^4
Intra-plate (*mid-plate*)	$v < 0.1$	$> 10^4$

After Scholz (1990).

estimated at $150 million and more than 600 fatalities. In the USA, three of the largest intra-plate earthquakes in modern record occurred in the mid-continent in 1811 and 1812. They caused significant ground effects in the New Madrid area of Missouri and were felt as far away as New England and Canada. From a tectonic standpoint, the occurrence of intra-plate earthquakes shows that the lithosphere is not rigid and internal fractures can take place; the latter are, however, difficult to predict. The genesis of this seismic activity is attributed either to the geological complexity of the lithosphere or anomalies in its temperature and strength. Stress build-ups at the edges may be transmitted across the plates and are released locally in weak zones of the crust. It has been shown that intra-plate events exhibit much higher stress drops than their inter-plate counterparts, the difference being a factor five (Scholz *et al.*, 1986). Intra-plate and inter-plate earthquakes can be distinguished quantitatively on the basis of the slip rate of their faults and the recurrence time (Scholz, 1990) as outlined in Table 1.1. For example, the Kashmir earthquake of 8 October 2005 is associated with the known subduction zone of an

active fault where the Eurasian and the Indian plates are colliding and moving northward at a rate of 40 mm/year (Durrani *et al.*, 2005). The data collected for the Kashmir earthquake correspond to the figures given in Table 1.1 for slip rate and recurrence time of a typical inter-plate seismic event.

Intra-plate earthquakes generally fall into two groups: plate boundary-related and mid-plate. The former take place either in broad bands near plate edges and are tectonically linked to them or in diffuse plate boundaries. Examples of such earthquakes have occurred inland in Japan, and are linked tectonically to the Pacific–Eurasian plate. In contrast, mid-plate earthquakes are not related to plate edges. Inter- and intra-plate crustal movements are continuously occurring and information concerning worldwide earthquake activity can be found at several Internet sites, for example http://www.usgs.gov, among others.

1.1.2 Faulting

When two ground masses move with respect to one another, elastic strain energy due to tectonic processes is stored and then released through the rupture of the interface zone. The distorted blocks snap back towards equilibrium and an earthquake ground motion is produced. This process is referred to as 'elastic rebound'. The resulting fracture in the Earth's crust is termed a 'fault'. During the sudden rupture of the brittle crustal rock seismic waves are generated. These waves travel away from the source of the earthquake along the Earth's outer layers. Their velocity depends on the characteristics of the material through which they travel. Further details on types of seismic waves are given in Section 1.1.3.

The characteristics of earthquake ground motions are affected by the slip mechanism of active faults. Figure 1.5 provides two examples of significant active faults: the San Andreas fault in California and the Corinth Canal fault in Greece, with about 70 m exposure height.

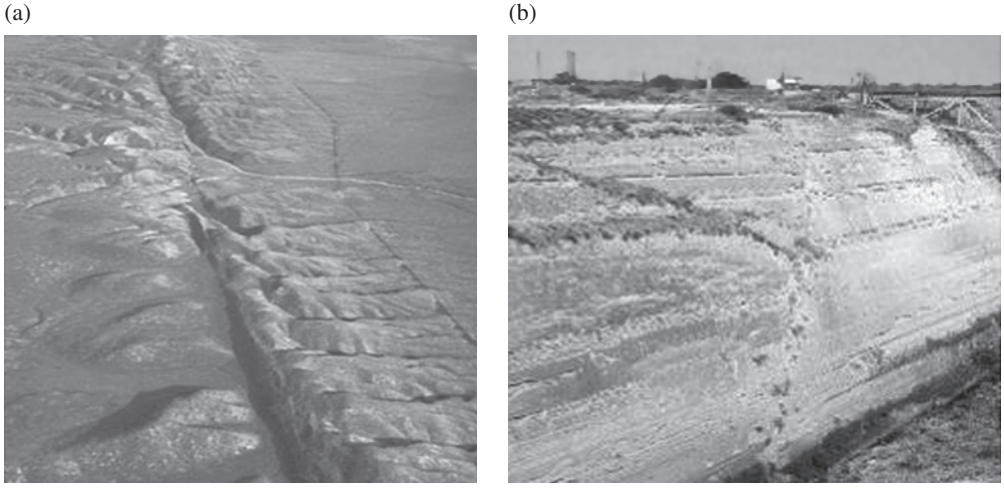

Figure 1.5 Active faults: San Andreas in California (a) and the Corinth Canal in Greece (b).

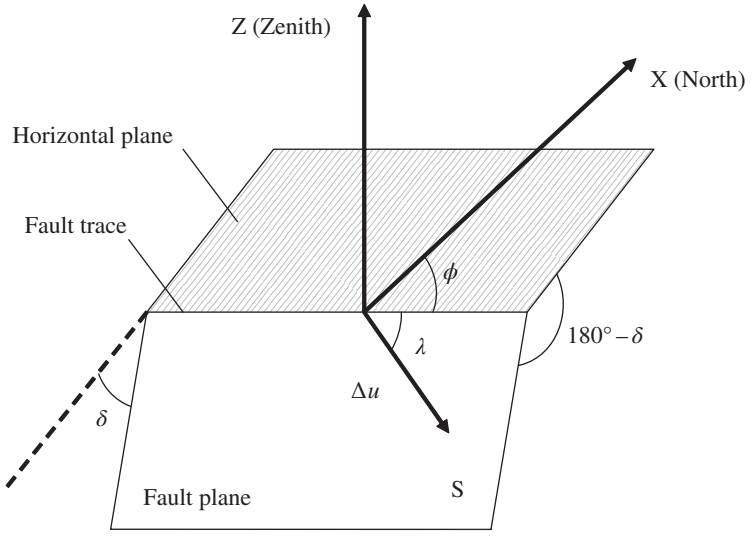

Figure 1.6 Parameters used to describe fault motion.

Active faults may be classified on the basis of their geometry and the direction of relative slip. The parameters used to describe fault motion and its dimensions are as follows:

(i) *Azimuth (ϕ):* the angle between the trace of the fault, that is the intersection of the fault plane with the horizontal, and the northerly direction ($0° \le \phi \le 360°$). The angle is measured so that the fault plane dips to the right-hand side.
(ii) *Dip (δ):* the angle between the fault and the horizontal plane ($0° \le \delta \le 90°$).
(iii) *Slip or rake (λ):* the angle between the direction of relative displacement and the horizontal direction ($-180° \le \lambda \le 180°$). It is measured on the fault plane.
(iv) *Relative displacement (Δu):* the distance travelled by a point on either side of the fault plane. If Δu varies along the fault plane, its mean value is generally used.
(v) *Area (S):* surface area of the highly stressed region within the fault plane.

The orientation of fault motion is defined by the three angles ϕ, δ and λ, and its dimensions are given by its area S as displayed in Figure 1.6; the fault slip is measured by the relative displacement Δu.

Several fault mechanisms exist depending on how the plates move with respect to one another (Housner, 1973). The most common mechanisms of earthquake sources are described below (Figure 1.7):

(i) *Dip-slip faults:* one block moves vertically with respect to the other. If the block underlying the fault plane or 'foot wall' moves up the dip and away from the block overhanging the fault plane or 'hanging wall', normal faults are obtained. Tensile forces cause the shearing failure of normal faults. In turn, when the hanging wall moves upward in relation to the foot wall the faults are reversed; compressive forces cause the failure. Thrust faults are reverse faults characterised by a very small dip. Mid-oceanic ridge

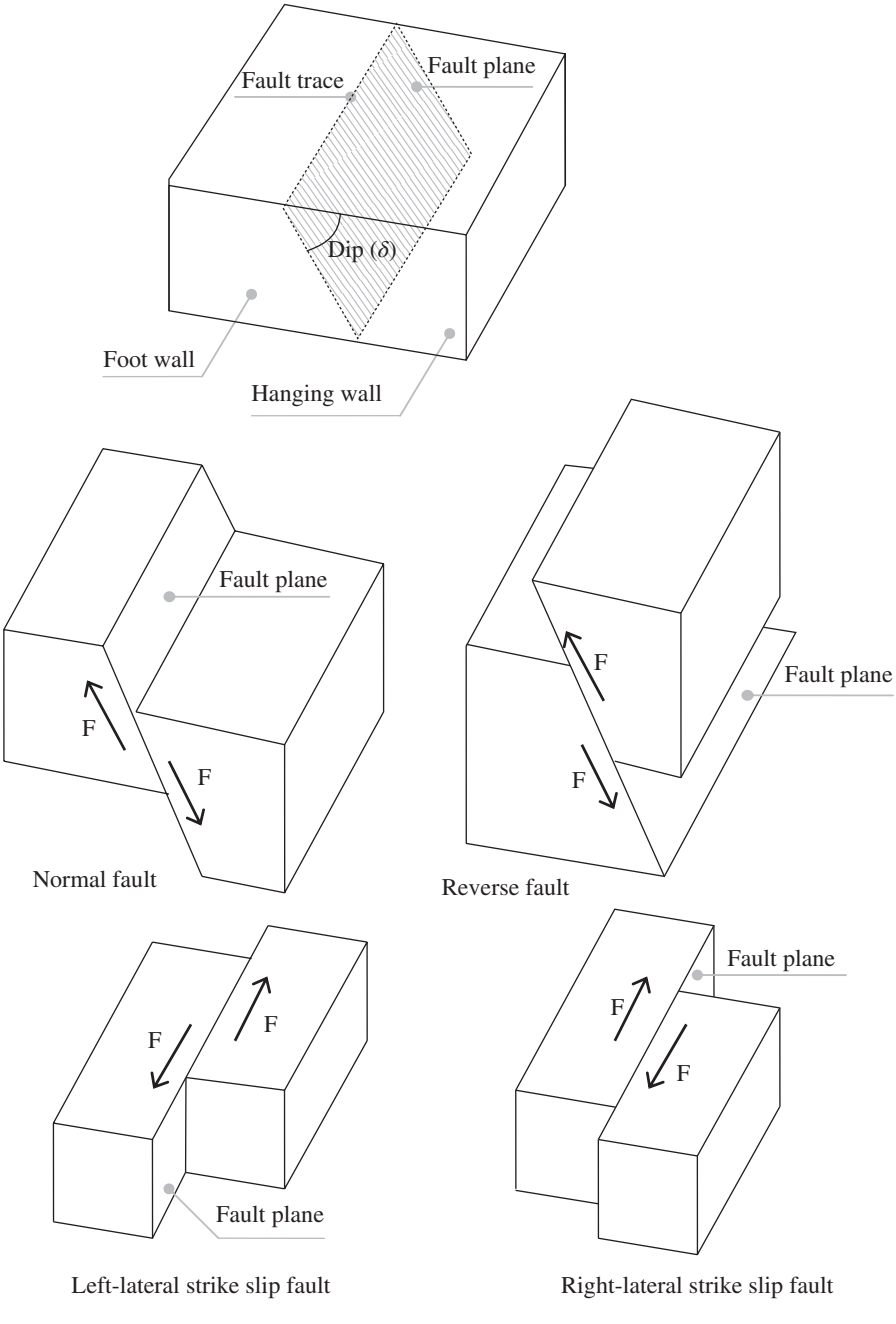

Figure 1.7 Fundamental fault mechanisms.

earthquakes are due chiefly to normal faults. The 1971 San Fernando earthquake in California was caused by rupture of a reverse fault. Earthquakes along the Circum-Pacific seismic belt are caused by thrust faults.

(ii) *Strike-slip faults:* the adjacent blocks move horizontally past one another. Strike-slip can be right-lateral or left-lateral, depending on the sense of the relative motion of the blocks for an observer located on one side of the fault line. The slip takes place along an essentially vertical fault plane and can be caused by either compression or tension stresses. They are typical of transform zones. An example of strike-slip occurred in the 1906 San Francisco earthquake on the San Andreas fault. The latter is characterised by large strike-slip deformations when earthquakes occur (see also Figure 1.5): part of coastal California is sliding to the northwest relative to the rest of North America – Los Angeles is slowly moving towards San Francisco.

Several faults exhibit combinations of strike-slip and dip-slip movements; the latter are termed 'oblique slip'. Oblique slips can be either normal or reverse and right- or left-lateral. The above fault mechanisms can be defined in mathematical terms through the values of the dip δ and the slip or rake λ. For example, strike-slip faults show $\delta = 90°$ and $\lambda = 0°$. The slip angle λ is negative for normal faults and positive for reverse faults; for $\delta > 0°$ the fault plane is inclined and can exhibit either horizontal ($\lambda = \pm 180°$ and $0°$) or vertical ($\lambda = \pm 90°$) motion. For other λ-values the relative displacement has both vertical and horizontal components; the latter can be of normal or reverse type according to the algebraic sign of the angle λ.

The 'focus' or 'hypocentre' of an earthquake is the point under the surface where the rupture is said to have originated. The projection of the focus on the surface is termed 'epicentre'. The reduction of the focus to a point is the point-source approximation (Mallet, 1862). This approximation is used to define the hypocentral parameters. However, the parameters that define the focus are similar to those that describe the fault fracture and motion. Foci are located by geographical coordinates, namely latitude and longitude, the focal depth and the origin or occurrence time. Figure 1.8 provides a pictorial depiction of the source parameters, namely epicentral distance, hypocentral or focal distance and focal depth. Earthquakes are

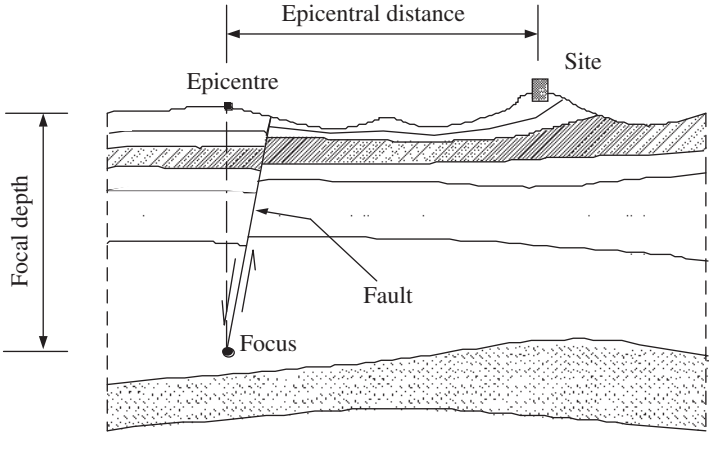

Figure 1.8 Definition of source parameters.

generated by sudden fault slips of brittle rocky blocks, starting at the focus depth and observed at a site located at the epicentral distance.

Most earthquakes have focal depths in the range of 5–15 km, while intermediate events have foci at about 20–50 km and deep earthquakes occur at 300–700 km underground. The three types are also referred to as shallow, intermediate and deep focus, respectively. Crustal earthquakes normally have depths of about 30 km or less. For example, in central California the majority of earthquakes have focal depths in the upper 5–10 km. Some intermediate- and deep-focus earthquakes are located in Romania, the Aegean Sea and under Spain.

The above discussion highlights one of the difficulties encountered in characterising earthquake parameters, namely the definition of the source. From Figure 1.8, it is clear that the source is not a single point, hence the 'distance from the source' required for engineering seismology applications, especially in attenuation relationships as discussed in Section 3.3, is ill-defined. This has led researchers to propose treatments for point, line and area sources (Kasahara, 1981). It is therefore important to exercise caution in using relationships based on source-site measurements, especially for near-field (with respect to site) and large magnitude events. A demonstration of this is the values of ground acceleration measured in the Adana–Ceyhan (Turkey) earthquake of 26 June 1998. Two seismological recording stations, at Ceyhan and Karatas, were located at distances of 32 and 36 km from the epicentre, respectively. Whereas the peak acceleration in Ceyhan was 0.27 g, that at Karatas was 0.03 g. The observed anomaly may be explained by considering the point of initiation and propagation of the fault rupture or 'directivity', which is presented in Section 1.3.1, possibly travelling towards Ceyhan and away from Karatas.

Problem 1.1

Determine the source mechanism of faults with a dip $\delta = 60°$ and rake $\lambda = 45°$. Comment on the results.

1.1.3 Seismic Waves

Fault ruptures cause brittle fractures of the Earth's crust and dissipate up to 10% of the total plate-tectonic energy in the form of seismic waves. Earthquake shaking is generated by two types of elastic seismic waves: body and surface waves. The shaking felt is generally a combination of these waves, especially at small distances from the source or 'near-field'.

Body waves travel through the Earth's interior layers. They include longitudinal or primary waves (also known as 'P-waves') and transverse or secondary waves (also called 'S-waves'). P- and S-waves are also termed 'preliminary tremors' because in most earthquakes they are felt first (Kanai, 1983). P-waves cause alternate push (or compression) and pull (or tension) in the rock as shown in Figure 1.9. Thus, as the waves propagate, the medium expands and contracts, while keeping the same form. They exhibit similar properties to sound waves, show small amplitudes and short periods and can be transmitted in the atmosphere. P-waves are seismic waves with relatively little damage potential. S-wave propagation, by contrast, causes vertical and horizontal side-to-side motion. Such waves introduce shear stresses in the rock along their paths as displayed in Figure 1.9 and are thus also defined as 'shear waves'. Their motion can be separated into horizontal (SH) and vertical (SV) components, both of which can

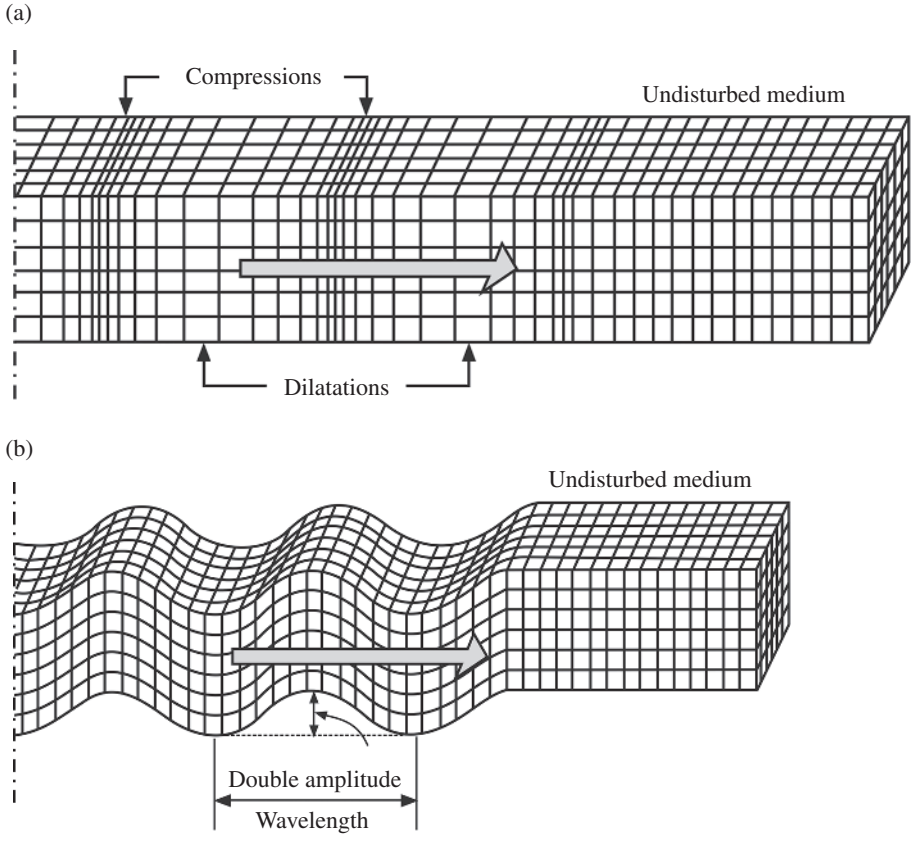

Figure 1.9 Travel path mechanisms of body waves: P- (a) and S-waves (b). (Adapted from Bolt, 1999).

cause significant damage, as illustrated in Sections 1.4.1 and 1.4.2 as well as in Appendix B. Shear waves are analogous to electromagnetic waves, show large amplitudes and long periods and cannot propagate in fluids.

Body waves (P and S) were named after their arrival time as measured by seismographs at observation sites. P-waves travel faster, at speeds between 1.5 and 8 km/s while S-waves are slower, usually travelling at 50–60% of the speed of P-waves. The actual speed of body waves depends upon the density and elastic properties of the rock and soil through which they pass.

Body waves may be described by Navier's equation for an infinite, homogeneous, isotropic, elastic medium in the absence of body forces (e.g. Udias, 1999). The propagation velocities of P- and S-waves within an isotropic elastic medium with density ρ, denoted as v_P and v_S respectively, are as follows:

$$v_P = \sqrt{\frac{E(1-\nu)}{\rho(1+\nu)(1-2\nu)}} \tag{1.1.1}$$

Table 1.2 Velocity of P- and S-waves in the Earth's layers.

Layer (type)	Depth (km)	P-waves (km/s)	S-waves (km/s)
Crust	10–30	6.57	3.82
	40	8.12	4.42
Upper mantle	220	8.06	4.35
	400	9.13	5.22
	670	10.75	5.95
Lower mantle	1200	11.78	6.52
	2885	13.72	7.26
	2890	8.06	0.00
Outer core	3800	9.31	0.00
	5150	10.36	0.00
Inner core	5155	11.03	3.50
	6371	11.26	3.67

$$v_S = \sqrt{\frac{E}{2\rho(1+\nu)}} \tag{1.1.2}$$

in which ν is Poisson's ratio and E is Young's modulus of the elastic medium.

The ratio of P- and S-wave velocities is as follows:

$$\frac{v_s}{v_P} = \sqrt{\frac{1-2\nu}{2(1-\nu)}} \tag{1.2.1}$$

and for ν-values characterising ordinary soil types, that is with ν ranging between 0.30 and 0.50:

$$0 \le v_s \le 0.53\, v_P \tag{1.2.2}$$

Equations (1.2.1) and (1.2.2) can be employed along with wave traces of seismogram records to locate earthquakes in time and space. For shallow earthquakes the effects of the Earth's curvature can be ignored and hence a planar model is used for the propagation of body waves. Assuming homogeneous soil profiles between earthquake foci and observation sites, the focal distance Δx is linearly dependent on the time-lag Δt between the P- and S-waves as follows:

$$\Delta x = \frac{v_P\, v_S}{v_P - v_S}\Delta t \tag{1.3.1}$$

thus, if the wave velocities v_p and v_S are known, the distance Δx is readily evaluated. Velocities of P- and S-waves in the Earth's interior layers are given in Table 1.2. For a quick evaluation, Omori's formula may also be used (Kanai, 1983):

$$\Delta x \approx 7.42\, \Delta t \tag{1.3.2}$$

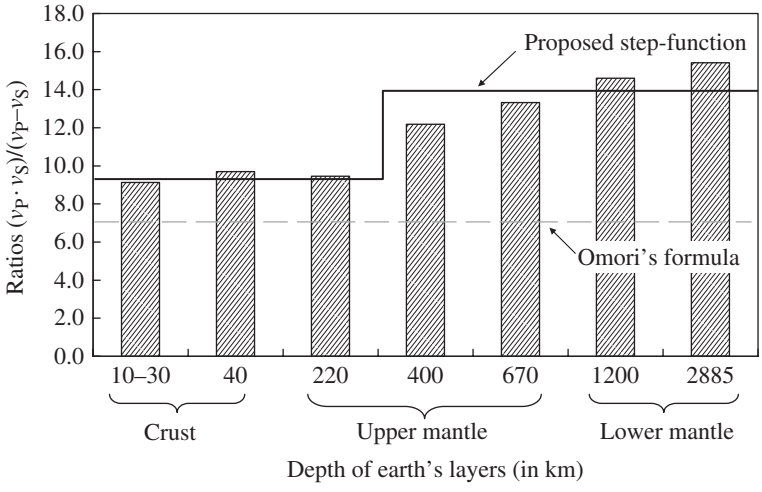

Figure 1.10 Comparison between ratios of body wave velocities in Eqs. (1.3.1) and (1.3.2).

with Δx and Δt expressed in kilometres and seconds, respectively. Equation (1.3.2) assumes that body wave velocities are almost constant within a limited area. A comparison between the coefficient '7.42' used by Omori in Eq. (1.3.2), the coefficients that are computed by using the first term on the right-hand side in Eq. (1.3.1) and the values of v_P and v_S given in Table 1.2 is provided in Figure 1.10. It is proposed to make use of a step-function to take into consideration the variability of the body wave velocities in the Earth's interior. The suggested coefficients for Eq. (1.3.2) are 9.43 and 13.88, for depths below and above 300 km, respectively.

The procedure to locate an earthquake epicentre and origin time, that is time of initiating of fault rupture, is as follows:

(a) Obtain seismogram records for a given observation site.
(b) Select the arrival time of the body waves on the record traces.
(c) Compute the time delay Δt in the arrival of P- and S-waves.
(d) Subtract the travel time Δt from the arrival time at the observation site to obtain the origin time.
(e) Use Eqs. (1.3.1) or (1.3.2) to evaluate the distance Δx between the seismic station and the epicentre. The use of either Eqs. (1.3.1) or (1.3.2) depends on the data available for the soil profile and approximation accepted.
(f) Draw a circle on a map around the station location (or centre) with a radius equal to Δx. The curve plotted shows a series of possible locations for the earthquake epicentre.
(g) Repeat steps (a) to (f) for a second seismic station. A new circle is drawn; the latter intersects the circle of the first station at two points.
(h) Repeat steps (a) to (f) for a third seismic station. It identifies which of the two previous possible points is acceptable and corresponds to the earthquake source.

Errors are common in the above graphical method; hence the procedure becomes more accurate with the increase in the number of measuring stations. In which case, the intersection

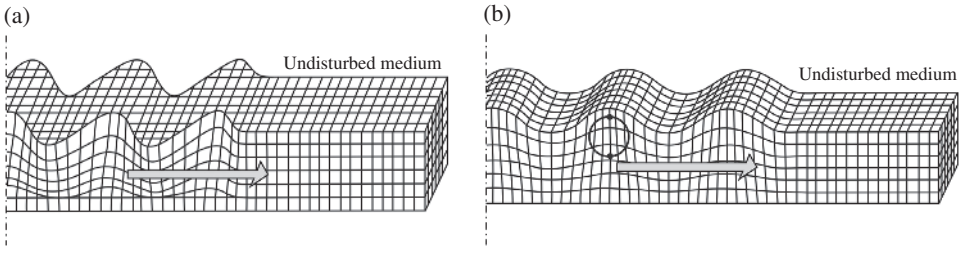

Figure 1.11 Travel path mechanisms of surface waves: Love (a) and Rayleigh waves (b). (Adapted from Bolt, 1999.)

will correspond to a small area containing the epicentre. In recent times, computer-based techniques have been employed to enhance the accuracy in evaluating earthquake epicentral locations (e.g. Lee *et al.*, 2003).

Equations (1.3.1) and (1.3.2) may be employed to derive travel–time curves, that is plots of the time seismic waves take to propagate from the earthquake source to each seismograph station or 'observation site', as a function of the horizontal distance. The use of these curves is twofold: estimating the Earth's internal structure and seismic prospecting (extensively used for underground structures). In particular, travel–time curves for earthquakes observed worldwide have shown that S-waves cannot travel deeper than 2900 km (reference is also made to Table 1.2). At this depth the medium has no rigidity and hence only P-waves can propagate through it.

Surface waves propagate across the outer layers of the Earth's crust. They are generated by constructive interference of body waves travelling parallel to the ground surface and various underlying boundaries. Surface waves include Love (indicated as 'L- or LQ-waves') and Rayleigh (indicated as 'R- or LR-waves') waves. These waves induce generally large displacements and hence are also called 'principal motion' (Kanai, 1983). They are most distinct at distances further away from the earthquake source. Surface waves are most prominent in shallow earthquakes while body waves are equally well represented in earthquakes at all depths. Because of their long duration, surface waves are likely to cause severe damage to structural systems during earthquakes.

LQ-waves are generated by constructive interference of SH body waves and hence cannot travel across fluids. Their motion is horizontal and perpendicular to the direction of their propagation, which is parallel to the Earth's surface as illustrated pictorially in Figure 1.11. LQ-waves have large amplitudes and long periods. LQ-waves of long period (60–300 seconds) are also called 'G-waves', after Gutenberg (Richter, 1958). For these periods the waves travel with a velocity of about 4.0 km/s and are pulse-like.

LR-waves are caused by constructive interference of body waves, such as P and SV. As they pass by, particles of soil move in the form of a retrograde ellipse whose long axis is perpendicular to the Earth's surface (Figure 1.11). R-waves exhibit very large amplitude and regular waveforms.

LR-waves are slower than S-waves. As an approximation, it may be assumed that the velocity of LR-waves v_{LR} is given by the equation (Bolt, 1999):

$$v_{LR} \approx 0.92\, v_S \tag{1.4}$$

For a layered solid, LQ-wave velocity v_{LQ} generally obeys the following relationship:

$$v_{S1} < v_{LQ} < v_{S2} \tag{1.5}$$

with v_{S1} and v_{S2} the velocities of S-waves in the surface and deeper layers, respectively.

Surface waves are slower than body waves and LQ-waves are generally faster than LR-waves. Moreover, the amplitudes of P- and S-waves show amplitudes linearly decreasing with the increase in distance x, while the amplitude of surface waves attenuate in inverse proportion to the square root of distance x. P-waves damp more rapidly than S-waves; attenuations increase with the wave frequencies. Amplitude attenuation is caused by the viscosity of the Earth's crust; seismic waves also change in form during their travel paths for the same reason (Kanai, 1983). Amplitudes and periods are of great importance because they influence the energy content of seismic waves as discussed in Section 1.2.

Body waves are reflected and refracted at interfaces between different layers of rock according to Snell's law of refraction. When reflection and refraction occur part of the energy of one type is transformed in the other. Regardless of whether the incident wave is P or S, the reflected and refracted waves, also termed 'multiple phase waves', each consist of P- and S-waves, such as PP, SS, PS and SP. Their name indicates the travel path and mode of propagation (Reiter, 1990). For example, SP starts as S and then continues as P. The phenomenon known as the 'Moho bounce' is due to the simultaneous arrival at the surface of direct S-waves and S-waves reflected by the so-called 'Mohorovicic discontinuity' – or 'Moho' in short – at the boundary between the crust and the underlying mantle in the internal structure of the Earth. The latter discontinuity may be responsible for significant strong motions leading to damage far from the source as illustrated in Section 1.2.1.

Multiple phase waves do not possess significant damage potential. However, when P- and S-waves reach the ground surface they are reflected back. As a result, waves move upwards and downwards. Such reflections may lead to significant local amplification of the shaking at the surface. It has been shown that seismic waves are influenced by soil conditions and local topography (e.g. Kramer, 1996), as further discussed in Section 1.3.2.

A final point worth noting about the various types of seismic waves is the likelihood of rotatory vibrations, also referred to as 'progressive waves', at ground surface. These waves occur in addition to translational oscillations and are generated either when a plane wave is incident obliquely to the ground surface or when surface waves are present. Progressive waves may excite rocking and torsional vibrations especially in high-rise structures (Okamoto, 1984). Rotatory earthquake motions are complex and not yet fully understood. They are subject to active research.

Problem 1.2

Locate and mark on the map provided in Figure 1.12 the epicentre of an earthquake that was recorded in Italy by three observation sites with a time delay between P- and S-waves of 5.0, 7.5 and 6.0 seconds, respectively. The body wave velocities are 8.5 and 4.30 km/s; it is up to the reader to determine which of these values refer to P- and S-waves. Compare the results obtained by Eq. (1.3.1) with those estimated from Eq. (1.3.2).

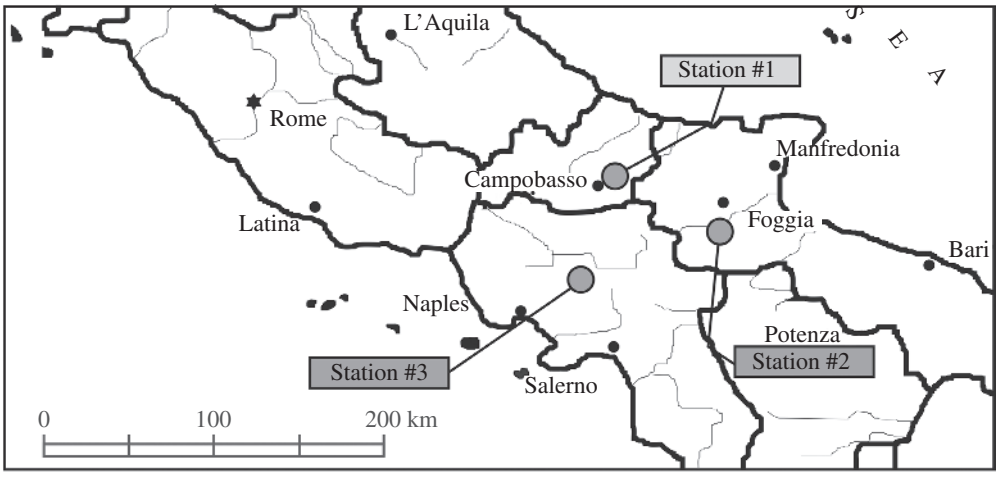

Figure 1.12 Map with the location of the seismological stations.

1.2 Measuring Earthquakes

Earthquake size is expressed in several ways. Qualitative or non-instrumental and quantitative or instrumental measurements exist; the latter can be either based on regional calibrations or applicable worldwide. Non-instrumental measurements are of great importance for pre-instrumental events and are hence essential in the compilation of historical earthquake catalogues for purposes of hazard analysis. For earthquakes that have been instrumentally recorded, qualitative scales are complementary to the instrumental data. The assessment and use of historical records is not straightforward and may lead to incorrect results due to inevitable biases (Ambraseys and Finkel, 1986). Moreover, the observation period during which data are employed to determine future projections is an issue of great importance. For example, recent studies (Ambraseys, 2006) indicate that for three active regions around the world, limiting the catalogues used in hazard analysis to a short period of time may grossly overestimate or underestimate the ensuing hazard. The over- and underestimation is a function of whether the observation period was an exceptionally quiescent or energetic epoch. Seismograms recorded at different epicentral distances are employed to determine origin time, epicentre, focal depth and type of faulting – as discussed in Sections 1.1.2 and 1.1.3 – as well as to estimate the energy released during an earthquake. Descriptive methods can also be used to establish earthquake-induced damage and its spatial distribution. In so doing, intensity, magnitude and relevant scales are utilised; these are outlined below.

1.2.1 Intensity

Intensity is a non-instrumental perceptibility measure of damage to structures, ground surface effects, for example fractures, cracks and landslides illustrated in Section 1.4.2, and human reactions to earthquake shaking. It is a descriptive method which has been traditionally used to establish earthquake size, especially for pre-instrumental events. It is a subjective damage

evaluation metric because of its qualitative nature, related to population density, familiarity with earthquake and type of constructions.

Discrete scales are used to quantify seismic intensity; the levels are represented by Roman numerals and each degree of intensity provides a qualitative description of earthquake effects. Several intensity scales have been proposed worldwide. Early attempts at classifying earthquake damage by intensity were carried out in Italy and Switzerland around the late 1700s and early 1900s (Kanai, 1983). Some of these scales are still used in Europe (alongside modern scales), the USA and Japan. Some of the most common intensity scales are listed below:

(i) *Mercalli–Cancani–Seiberg* (MCS): 12-level scale used in Southern Europe.
(ii) *Modified Mercalli* (MM): 12-level scale proposed in 1931 by Wood and Neumann, who adapted the MCS scale to the California data set. It is used in North America and several other countries.
(iii) *Medvedev–Sponheuer–Karnik* (MSK): 12-level scale developed in Central and Eastern Europe and used in several other countries.
(iv) *European Macroseismic Scale* (EMS): 12-level scale adopted since 1998 in Europe. It is a development of the MM scale.
(v) *Japanese Meteorological Agency* (JMA): 7-level scale used in Japan. It has been revised over the years and has recently been correlated to maximum horizontal acceleration of the ground.

Descriptions of the above intensity scales can be found in several textbooks (Reiter, 1990; Kramer, 1996; Lee *et al.*, 2003, among many others). A comparison between MCS, MM, MSK, EMS and JMA scales is provided in Figure 1.13. Intensity scales may include description of construction quality for structures in the exposed region. For example, the MM scale specifies different damage levels depending on whether the structural system was poorly built or badly designed (VII), ordinary substantial buildings (VIII) or structures built especially to withstand earthquakes (IX). However, intensity scales do not account for local soil conditions which may significantly affect the earthquake-induced damage and its distribution. Correlations between earthquake source and path, on the one hand, and intensity measures on the other are therefore highly inaccurate.

Intensity scales are used to plot contour lines of equal intensity or 'isoseismals'. Intensity maps provide approximate distributions of damage and the extent of ground shaking. Maps of local site intensity include reports of all observation sites and whether or not the strong motion was felt. For example, the isoseismal map of the 17 October 1989 Loma Prieta earthquake in California shown in Figure 1.14 locates the epicentre (marked as a star) and provides MM intensities between isoseismals (Roman numerals), and MM intensities at specific cities (Arabic numerals). The MM intensity of VIII was assigned to an area of about 50 km long and 25 km wide. Significant ground motions were generated at distances of several tens of kilometres from the earthquake source because of the Moho bounce and the soft soil amplifications, described in Sections 1.1.3 and 1.3.2, respectively.

Anomalous damage distributions may derive from the lack of populated areas in the neighbourhood of the epicentral regions, the depth of soil, local site conditions and directivity effects. Intensity value I_o at the epicentre, or 'epicentral intensity', is equal to the maximum

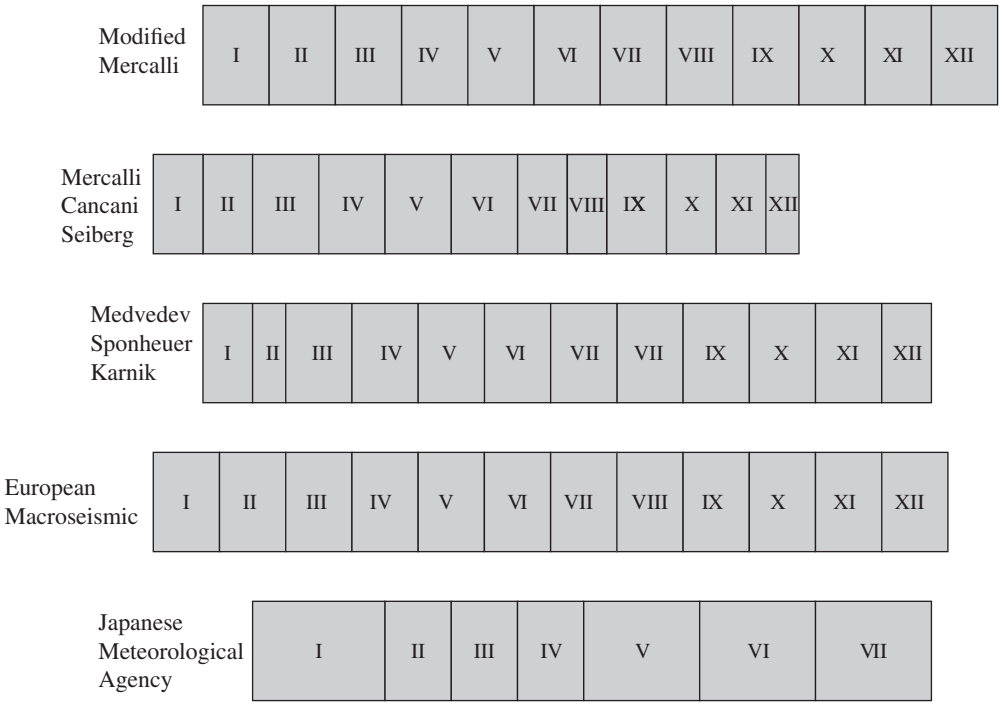

Figure 1.13 Comparison between seismic intensity scales.

intensity I_{max} felt during ground motion. However, for offshore earthquakes I_{max} is recorded on the coast and hence does not correspond to I_o.

In some scales, for example JMA, the intensity of earthquakes can also be expressed by the radius R of the felt area (Kanai, 1983). The relationship between R and the earthquake classification is provided in Table 1.3. Epicentral regions in perceptible earthquakes experience ground motions ranked not less than intensity V in the JMA scale.

It has been observed repeatedly that structures in the immediate vicinity of earthquake sources experience very high ground accelerations but sustain little or no damage (e.g. Elnashai *et al*., 1998). On the other hand, intensity is a measure of the perceptibility of the earthquake and its actual consequential damage. Therefore, relating intensity to peak ground acceleration is, in principle, illogical. However, the necessity of bridging the distance between historical earthquake observations (based mainly on intensity) and code-defined forces (based entirely on peak ground acceleration or displacement) warrants the efforts expended in correlating the two measures. Attenuation relationships correlating intensity and peak ground accelerations, which are presented in Section 3.3, do not reflect parameters influencing earthquake damage potential other than intensity, for example site amplification effects and directivity discussed in Sections 1.3.1 and 1.3.2. In addition, source characteristics and mechanisms do not affect intensity scales. The measurement of earthquake size should be based on the amount of energy released at the focus. Therefore, magnitude scales have been defined as presented hereafter.

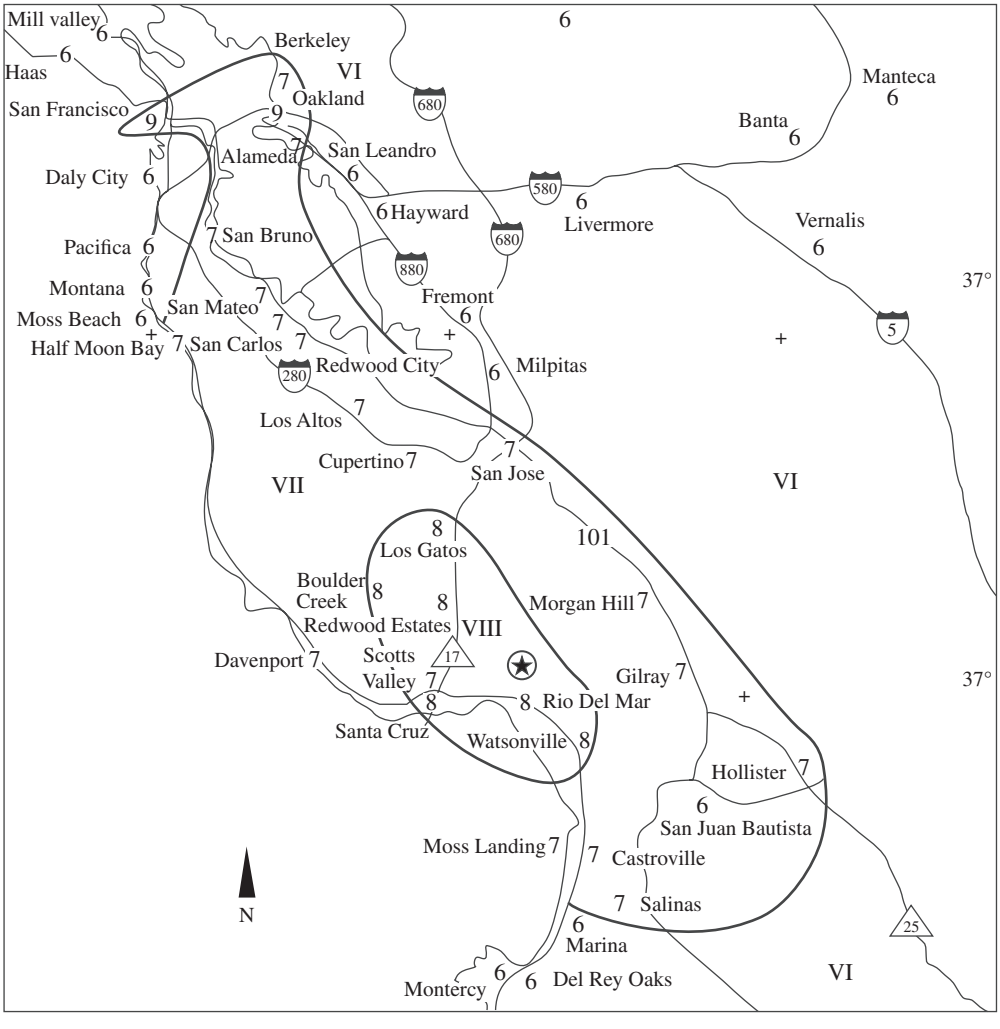

Figure 1.14 Isoseismal map for 1989 Loma Prieta earthquake in California. (After Plafker and Galloway, 1989.)

Table 1.3 Earthquake intensity based on the radius (R) of felt area.

Radius (km)	Earthquake intensity
$R < 100$	Local
$100 < R < 200$	Small region
$200 < R < 300$	Rather conspicuous
$R > 300$	Conspicuous

1.2.2 Magnitude

Magnitude is a quantitative measure of earthquake size and fault dimensions. It is based on the maximum amplitudes of body or surface seismic waves. It is therefore an instrumental, quantitative and objective scale. The first attempts to define magnitude scales were made in Japan by Wadati and in California by Richter in the 1930s. Several scales exist. Many of these scales are frequency-dependent because they measure amplitudes of seismic waves with different properties. Scales related directly to source parameters have also been proposed. These do not depend on specific waves and hence are frequency-independent. The most common magnitude scales are described herein:

(i) *Local (or Richter) magnitude (M_L):* measures the maximum seismic wave amplitude A (in microns) recorded on standard Wood–Anderson seismographs located at a distance of 100 km from the earthquake epicentre. The standard Wood–Anderson seismograph has a natural period of 0.8 seconds, a critical damping ratio of 0.8 and an amplification factor of 2800. It amplifies waves with periods between approximately 0.5 and 1.5 seconds, that is wavelengths of 500 m to 2 km. These waves are of particular interest for earthquake engineers due to their potential to cause damage. Magnitude M_L is related to A by the following relationship:

$$M_L = \log(A) - \log(A_0) \tag{1.6}$$

where A_0 is a calibration factor that depends on distance (Richter, 1958). The Richter scale was calibrated assuming that magnitude $M_L = 3$ corresponds to an earthquake at a distance of 100 km with maximum amplitude of $A = 1.0$ mm. Indeed, $\log A_0 = -3$ for a distance $D = 100$ km. Earthquakes with M_L greater than 5.5 cause significant damage, while an earthquake of $M_L = 2$ is the smallest event normally felt by people.

(ii) *Body wave magnitude (m_b):* measures the amplitude of P-waves with a period of about 1.0 second, that is less than 10 km wavelengths. This scale is suitable for deep earthquakes which have few surface waves. Moreover, m_b can measure distant events, for example epicentral distances not less than 600 km. Furthermore, P-waves are not affected by the depth of energy source. Magnitude m_b is related to the amplitude A and period T of P-waves as follows:

$$m_b = \log\left(\frac{A}{T}\right) + \sigma(\Delta) \tag{1.7}$$

in which $\sigma(\Delta)$ is a function of the epicentre distance Δ (in degrees). For example, if $\Delta = 45°$ then $\sigma = 6.80$; other values can be found in the literature (e.g. Udias, 1999).

(iii) *Surface wave magnitude (M_S):* is a measure of the amplitudes of LR-waves with a period of 20 seconds, that is wavelength of about 60 km, which are common for very distant earthquakes, for example where the epicentre is located at more than 2000 km. M_S is used for large earthquakes. However, it cannot be used to characterise deep or relatively small, regional earthquakes. This limitation is due to the characteristics of

LR-waves as described in Section 1.1.3. The relationship between amplitude A, period T, distance Δ and M_S is given by:

$$M_S = \log\left(\frac{A}{T}\right) + 1.66\log(\Delta) + 3.30 \tag{1.8}$$

where Δ is measured in degrees, the ground motion amplitude in microns and the period in seconds. Equation (1.8) is applicable for $\Delta > 15°$.

(iv) *Moment magnitude (M_W):* accounts for the mechanism of shear that takes place at earthquake sources. It is not related to any wavelength. As a result, M_w can be used to measure the whole spectrum of ground motions. Moment magnitude is defined as a function of the seismic moment M_0. This measures the extent of deformation at the earthquake source and can be evaluated as follows:

$$M_0 = G\,A\,\Delta u \tag{1.9.1}$$

in which G is the shear modulus of the material surrounding the fault, A is the fault rupture area and Δu is the average slip between opposite sides of the fault. The modulus G can be assumed to be 32 000 MPa in the crust and 75 000 MPa in the mantle. M_w is thus given by:

$$M_w = 0.67\log(M_0) - 10.70 \tag{1.9.2}$$

where M_0 is expressed in ergons.

Richter magnitude M_L exhibits several limitations. It is applicable only to small and shallow earthquakes in California and for epicentral distances less than 600 km. It is, therefore, a regional (or local) scale, while m_b, M_S and M_w are worldwide scales. The main properties of the above magnitude scales are summarised in Table 1.4. The mathematical definition of magnitude implies that all the above scales have virtually no upper and lower bounds.

Table 1.4 Properties of major magnitude scales.

Scale type	Author	Earthquake size	Earthquake depth	Epicentre distance	Reference parameter	Applicability	Saturation
M_L	Richter (1936)	Small	Shallow	<600 km	Wave amplitude	Regional (California)	✓
m_b	Gutenberg and Richter (1956a)	Small-to-medium	Deep	>1000 km	Wave amplitude (P-waves)	Worldwide	✓
M_s	Gutenberg and Richter (1936)	Large	Shallow	>2000 km	Wave amplitude (LR-waves)	Worldwide	✓
M_w	Kanamori (1977)	All	All	All	Seismic moment	Worldwide	n.a.

n.a. = not applicable and ✓ = saturation occurs.

Notwithstanding, the upper bound is provided by strength of materials in the Earth's crust and the characteristics of the waves measured, while minimum values of magnitude that may be recorded by sensitive seismographs are around −2. As a general guideline, earthquakes with magnitude between 4.5 and 5.5 can be defined as local, while large seismic events generally have a magnitude 6.0–7.0. Great earthquakes are those with magnitude larger than 7.0.

Other magnitude scales exist; they are usually based on maximum amplitudes A of certain waves recorded by seismographs. The general correlation between magnitude M and A is as follows (Reiter, 1990):

$$M = \log(A) + f(d,h) + C_S + C_R \tag{1.10}$$

in which the function $f(d,h)$ accounts for epicentral distance d and focal depth h. The coefficients C_S and C_R are station and regional corrections, respectively. They are introduced to account for local and regional effects.

Conversions between different magnitude scales can be performed using simple empirical or semi-empirical relations. For example, the M_{JMA}, which is a long-period measurement adopted by the JMA, is related to Richter magnitude M_L (Kanai, 1983) by the relationship:

$$M_{JMA} = 2.0\,M_L - 9.7 \tag{1.11}$$

where magnitude M_L is expressed in ergons.

Earthquakes of different size and energy release may have the same magnitude. Typical examples are the 1906 San Francisco (California) and the 1960 Chile earthquakes. Both events showed $M_S = 8.3$. However, the fault rupture area in Chile was about 35 times greater than that observed in California. Different fault rupture lengths correspond to different amounts of energy released; moment magnitude accounts for the extent of fault rupture (Scholz, 1990). The moment magnitude M_w is about 8 for the San Francisco fault while the Chile earthquake has a moment magnitude M_w of 9.5. Magnitude scales do not increase monotonically with earthquake size. This observation is known as 'saturation' and affects all scales which are related to seismic waves of a particular period and wavelength, that is frequency-dependent scales. Figure 1.15 shows a comparison between different magnitude scales. Saturation is evident as M_w increases ($M_w > 6.5$). Another magnitude scale, m_B, is included in the plot; m_B is a body wave scale measuring different types of body waves with periods between 1.0 and 10 seconds and is distinct from m_b.

For values of magnitude of about 5.5, scales m_b and M_S coincide; for smaller earthquakes, for example $M_w < 5.5$, $m_b > M_S$, while for large magnitude $M_S > m_b$. Thus, surface wave magnitudes underestimate the size of small earthquakes while they overestimate the size of large events. Magnitudes m_b and M_S saturate at about 6.5 and 8.5, respectively. The Richter scale stops increasing at $M_w = 7.0$. M_w does not suffer from saturation problems in the practical range of magnitude, of $2 < M_w < 10$. Therefore, it can be employed for all magnitudes. For shallow earthquakes, Bolt (1999) suggests using M_D, also referred to as 'coda-length magnitude', for magnitudes less than 3, either M_L or m_b for magnitudes between 3 and 7 and M_S for magnitudes between 5 and 7.5. The 1994 Northridge earthquake has been ranked, for example as 6.4 in the local magnitude scale M_L, 6.6 in M_S and 6.7 in M_w (Broderick *et al.*, 1994). At these magnitudes, the different scales provide similar values, as displayed, for example in Figure 1.15.

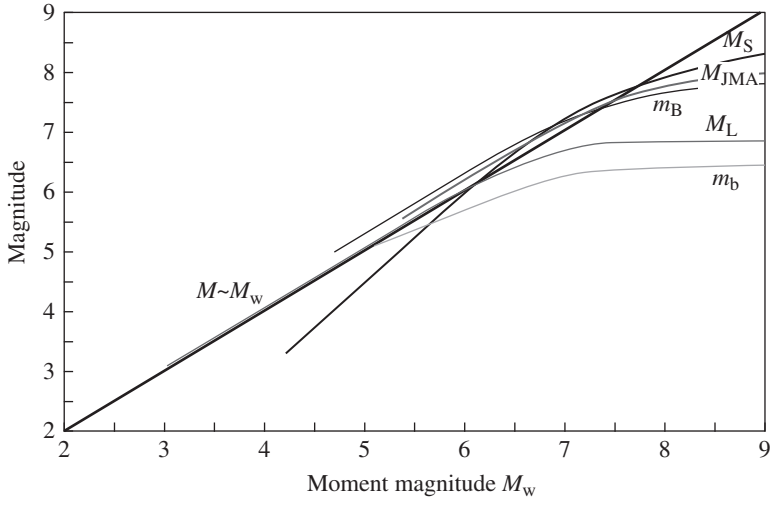

Figure 1.15 Saturation of magnitude scales.

Earthquake magnitude can be used to quantify the amount of energy released during fault ruptures. Energy propagating by seismic waves is proportional to the square root of amplitude–period ratios. Magnitude is proportional to the logarithm of seismic energy E. A semi-empirical relationship between surface wave magnitude M_S and E was formulated by Richter and Gutenberg (Richter, 1958), and is given by:

$$\log(E) = 1.5 M_S + 11.8 \tag{1.12}$$

where E is in ergons. As the magnitude increases by one unit, the energy increases by a factor of 31.6 and the difference between two units of magnitude is a factor of 1000 on energy release. Similarly, m_b and M_S are related to seismic energy E by the following empirical relations:

$$\log(E) = 2.4 m_b - 1.3 \tag{1.13.1}$$

$$\log(E) = 1.5 M_S + 4.2 \tag{1.13.2}$$

where E is expressed in joules (1 J = 10^7 ergs). Figure 1.16 indicates the correlation between surface wave magnitude M_S and energy released during earthquakes and other events. The number of earthquakes per year is also provided.

Seismic moment M_0 measures the energy E released by fault rupture during earthquakes (Scholz, 1990). The following relationship is applicable to all source mechanisms:

$$E = \frac{\Delta\tau}{2G} M_0 \tag{1.14}$$

where $\Delta\tau$ is the stress drop $\Delta\tau = \tau_1 - \tau_2$ and τ_1 and τ_2 and are the shear stresses on the fault before and after brittle fracture occurs, respectively; G is the shear modulus of the material surrounding

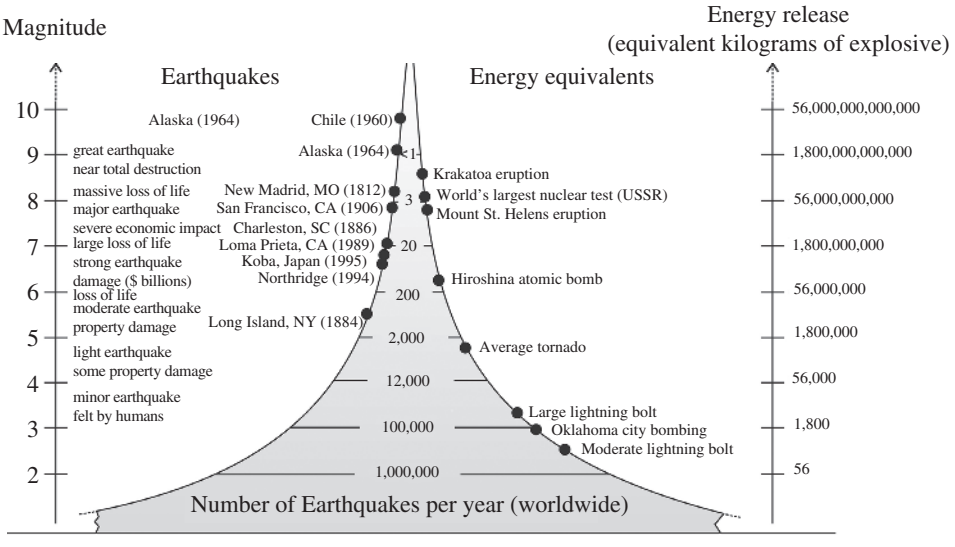

Figure 1.16 Correlation between magnitude and energy release. (After Bolt, 1999).

the fault as also shown in Eq. (1.9.1). For moderate-to-large earthquakes the mean values of $\Delta\tau$ are equal to about 6.0 MPa. In the definition of M_w the stress drop is assumed constant.

Magnitude–moment relationships have been defined empirically for periods less than 20 seconds (Purcaru and Berckhemer, 1978), as below:

$$\log\left(M_0\right) = 1.5\,M_S + 16.1 \tag{1.15}$$

and body wave magnitude m_b can be related over a wide range to M_S by the following semi-empirical formula proposed by Gutenberg and Richter (see Richter, 1958):

$$m_b = 0.63\,M_S + 2.5 \tag{1.16}$$

therefore, combining Eqs. (1.15) and (1.16), seismic moment M_0 can be related to body waves m_b and vice versa. Moreover, Figure 1.15 may be used when relationships between M_0 and magnitude scales other than m_b and M_S are sought.

Expressions correlating magnitude scales and fault rupture parameters can be found in the literature (e.g. Tocher, 1958; Housner, 1965; Seed *et al*., 1969; Krinitzsky, 1974; Mark and Bonilla, 1977). For example, Bonilla *et al*. (1984) computed M_S as a function of the fault rupture length L:

$$M_S\left(L\right) = 6.04 + 0.71\ \log\left(L\right) \tag{1.17.1}$$

where the length is in kilometres. Equation (1.17.1), which is applicable for $M_S > 6.7$, is based on mean values, while the 95th percentile is given as follows:

$$M_S^{0.95} = M_S\left(L\right) + 0.52 \tag{1.17.2}$$

Table 1.5 Values of coefficients in Eq. (1.18).

Fault mechanism	a	b
Normal	6.67	0.75
Reverse	6.79	1.31
Strike-slip	6.97	0.80

Surface wave magnitude M_S has also been related to the maximum observed displacement of fault D. Empirical relationships are provided as a function of the fault rupture mechanism (Slemmons, 1977), as shown below:

$$M_S = a + b\log(D) \tag{1.18}$$

where the displacement D is in metres, while coefficients a and b are given in Table 1.5.

Similarly, Wyss (1979) proposed a relationship between the fault surface rupture S and surface magnitude M_S given by:

$$M_S = 4.15 + \log(S) \tag{1.19}$$

in which the area S should be expressed in square kilometres. Equation (1.19) is applicable for $M_S > 5.6$.

In some regions, correlations as given above are of little value since many of the important geological features can be deeply buried by weathered materials. Results of studies by Wells and Coppersmith (1994) are outlined in Table 1.6 for different types of fault mechanisms, that is strike slip, reverse and normal. It was observed that large scatter may characterise the relationship between moment magnitude M_w and surface rupture length L (in kilometres), the subsurface rupture length L' (in kilometres), the rupture area A (in square kilometres), the downdip rupture width W (in kilometres, the maximum D and the average $\bar{D}$ surface displacement (in metres), especially for reverse-slip earthquakes.

Equations (1.17.1) and (1.17.2) and those in Table 1.6 are valid for earthquakes on or closer to tectonic place boundaries (inter-plate earthquakes). For earthquakes distant from plate boundaries (intra-plates events), such as the New Madrid seismic zone, a study by Nuttli (1983) showed that the latter equations may overestimate fault rupture lengths. Average source parameters and relevant magnitude scales are summarised in Table 1.7.

Differences between the values predicted by Eq. (1.17.1) and those provided in Table 1.7 drop as the rupture length increases. For short rupture lengths, for example 2–5 km, the variations exceed 50%, while for longer fault ruptures the differences are between 10% and 20%.

1.2.3 Intensity–Magnitude Relationships

Intensity–magnitude relationships are essential for the use of historical earthquakes for which no instrumental records exist. Several simple methods to convert intensity into magnitude have been proposed (e.g. Lee *et al.*, 2003); most of which exhibit large scatter because of the inevitable bias present in the definition of intensity (Ambraseys and Melville, 1982). Gutenberg

Table 1.6 Empirical relationships between moment magnitude M_w, surface rupture length L (km), subsurface rupture length L' (km), rupture area A (km^2), maximum D and average $\bar{D}$ surface displacement, in metres.

Fault mechanism	Relationship	σ_{M_w}	Relationship	$\sigma_{\log L,A,D}$	Magnitude range	Length/width/ displacement range (km)
Strike slip	$M_w = 5.16 + 1.12 \log L$	0.28	$\log L = 0.74 M_w - 3.55$	0.23	5.6–8.1	1.3–432
Reverse	$M_w = 5.00 + 1.22 \log L$	0.28	$\log L = 0.63 M_w - 2.86$	0.20	5.4–7.4	3.3–85
Normal	$M_w = 4.86 + 1.32 \log L$	0.34	$\log L = 0.50 M_w - 2.01$	0.21	5.2–7.3	2.5–41
All	$M_w = 5.08 + 1.16 \log L$	0.28	$\log L = 0.69 M_w - 3.22$	0.22	5.2–8.1	1.3–432
Strike-slip	$M_w = 4.33 + 1.49 \log L'$	0.24	$\log L' = 0.62 M_w - 2.57$	0.15	4.8–8.1	1.5–350
Reverse	$M_w = 4.49 + 1.49 \log L'$	0.26	$\log L = 0.58 M_w - 2.42$	0.16	4.8–7.6	1.1–80
Normal	$M_w = 4.34 + 1.54 \log L'$	0.31	$\log L' = 0.50 M_w - 1.88$	0.17	5.2–7.3	3.8–63
All	$M_w = 4.38 + 1.49 \log L'$	0.26	$\log L' = 0.59 M_w - 2.44$	0.16	4.8–8.1	1.1–350
Strike-slip	$M_w = 3.98 + 1.02 \log A$	0.23	$\log A = 0.90 M_w - 3.42$	0.22	4.8–7.9	3–5184
Reverse	$M_w = 4.33 + 0.90 \log A$	0.25	$\log A = 0.98 M_w - 3.99$	0.26	4.8–7.6	2.2–2400
Normal	$M_w = 3.93 + 1.02 \log A$	0.25	$\log A = 0.82 M_w - 2.87$	0.22	5.2–7.3	19–900
All	$M_w = 4.07 + 0.98 \log A$	0.24	$\log A = 0.91 M_w - 3.49$	0.24	4.8–7.9	2.2–5184
Strike-slip	$M_w = 3.80 + 2.59 \log W$	0.45	$\log W = 0.27 M_w - 0.76$	0.45	4.8–8.1	1.5–350
Reverse	$M_w = 4.37 + 1.95 \log W$	0.32	$\log W = 0.41 M_w - 1.61$	0.32	4.8–7.6	1.1–80
Normal	$M_w = 4.04 + 2.11 \log W$	0.31	$\log W = 0.35 M_w - 1.14$	0.31	5.2–7.3	3.8–63
All	$M_w = 4.06 + 2.25 \log W$	0.41	$\log W = 0.32 M_w - 1.01$	0.41	4.8–8.1	1.5–350
Strike-slip	$M_w = 6.81 + 0.78 \log D$	0.29	$\log D = 1.03 M_w - 7.03$	0.34	5.6–8.1	0.01–14.6
Reverse[a]	$M_w = 6.52 + 0.44 \log D$	0.52	$\log D = 0.29 M_w - 1.84$	0.42	5.4–7.4	0.11–6.5
Normal	$M_w = 6.61 + 0.71 \log D$	0.34	$\log D = 0.89 M_w - 5.90$	0.38	5.2–7.3	0.06–6.1
All	$M_w = 6.69 + 0.74 \log D$	0.40	$\log D = 0.82 M_w - 5.46$	0.42	5.2–8.1	0.01–14.6
Strike-slip	$M_w = 7.04 + 0.89 \log \bar{D}$	0.28	$\log \bar{D} = 0.90 M_w - 6.32$	0.28	5.6–8.1	0.05–8.0
Reverse[a]	$M_w = 6.64 + 0.13 \log \bar{D}$	0.50	$\log \bar{D} = 0.08 M_w - 0.74$	0.38	5.8–7.4	0.06–1.5
Normal	$M_w = 6.78 + 0.65 \log \bar{D}$	0.33	$\log \bar{D} = 0.63 M_w - 4.45$	0.33	6.0–7.3	0.08–2.1
All	$M_w = 6.93 + 0.82 \log \bar{D}$	0.39	$\log \bar{D} = 0.69 M_w - 4.80$	0.36	5.6–8.1	0.05–8.0

[a] Regression relationships are not statistically significant at a 95% probability level.
After Wells and Coppersmith (1994).

and Richter (1956) proposed a linear relationship between local magnitude M_L and epicentral intensity I_0 for southern California, given by:

$$M_L = 0.67 I_0 + 1.00 \tag{1.20}$$

in which the intensity I_0 is expressed in the MM scale. The above equation shows, for example, that the epicentral intensity I_0 of VI corresponds to $M_L = 5.02$ indicating that the earthquake is likely to cause significant damage.

Table 1.7 Average source parameters for mid-plate earthquakes.

Rupture length (km)	Slip (m)	m_b	M_S	log M_0 (dyne-cm)
2.1	0.01	4.5	3.35	22.2
3.8	0.03	5.0	4.35	23.2
7.0	0.11	5.5	5.35	24.2
13.0	0.34	6.0	6.35	25.2
24.0	1.10	6.5	7.35	26.2
45.0	3.70	7.0	8.32	27.2
58.0	5.80	7.2	8.53	27.6
75.0	9.20	7.4	8.87	28.0
85.0	11.50	7.5	9.00	28.2

After Nuttli (1983).

Street and Turcotte (1977) related m_b magnitude to the intensity I_0 (in the MM scale) as follows:

$$m_b = 0.49\, I_0 + 1.66 \tag{1.21}$$

which is useful in converting earthquake data in the central and eastern USA. Equation (1.21) relates an intensity of VI in the MM scale to a magnitude m_b of 4.60, which contradicts the observation that M_L should be systematically lower than m_b for short-period waves, as discussed in Section 1.2.2. This contradiction may be due to different rates of earthquake occurrence in various regions of the USA (Reiter, 1990). It also demonstrates that values obtained from intensity–magnitude relationships should be subject to engineering judgement. Regression analyses carried out on magnitudes predicted by Eqs. (1.20) and (1.21) and values measured for the same events have in many instances indicated poor statistical correlations. For example, correlation coefficients as low as ~0.5 are obtained when comparing earthquakes which occurred between the 1930s and 1970s in Quebec (Canada) and some regions of the USA, such as Illinois and New York (Reiter, 1990). As a result, several other methods have been proposed in an attempt to correlate intensity and magnitude scales. These formulations have been based on different intensity-related parameters, such as the felt area, the area inscribed by intensity IV isoseismals and the fall-off of intensity with distance.

Intensity–magnitude relationships were proposed by Ambraseys (1985, 1989) for European regions as follows:

$$M_S = -1.10 + 0.62\, I_i + 1.30 \cdot 10^{-3}\, r_i + 1.62 \log\left(r_i\right) \tag{1.22.1}$$

which is applicable for northwest Europe, and

$$M_S = -0.90 + 0.58\, I_i + 1.10 \cdot 10^{-3}\, r_i + 2.11 \log\left(r_i\right) \tag{1.22.2}$$

for the Alpine zone, where I_i is the MM intensity of the ith isoseismal and r_i is the radius of equivalent area enclosed by the ith isoseismal, in kilometres.

Local geological conditions and focal depths can significantly affect the intensity of earthquake ground motion. Semi-empirical formulations accounting for focal depths are available (e.g. Kanai, 1983). Sponheuer (1960) proposed to calculate M from the epicentral intensity I_0 as follows:

$$M_S = 0.66\, I_0 + 1.70 \log(h) - 1.40 \tag{1.23}$$

where the focal depth h is in kilometres and the intensity I_0 is in the MM scale.

Attenuation relationships (relationships between a ground-shaking parameter, magnitude, distance and soil condition) for different ground-motion parameters can be derived from intensity and magnitude; they may account for distance, travel path and site effects. The most common attenuation relationships formulated for active seismic regions worldwide are presented in Section 3.3.

Problem 1.3

Calculate the surface wave magnitude M_S for an earthquake with I_{MM} of VII, in an area that can be approximated by a circle with radius 20 km for a site at the borders of the given isoseismal. This site is located in the western United States but you may use Eq. (1.22.1). Compare the ensuing value with the estimations from relationships with other magnitude scales. Calculate the fault surface displacements. Assume that the earthquake mechanism is normal faulting.

1.3 Source-to-Site Effects

The characteristics of seismic waves are altered as they travel from the source to the site of civil engineering works, due to wave dispersion at geological interfaces, damping and changes in the wavefront shape. The latter are referred to as 'distance and travel path effects'. Moreover, local site conditions may affect significantly the amplitude of earthquake ground motions; these are known as 'site effects'. Non-linearity of soil response and topographical effects may also influence ground-motion parameters (Silva, 1988) as shown in Table 1.8. For example, during the 26 September 1997 Umbria-Marche (Italy) earthquake, significant site amplification was observed even at large distances from the epicentre (Sano and Pugliese, 1999). Due to the geomorphological conditions in the epicentral area, located in the Apennines, local soil amplifications related both to topographical and basin effects were present. During the long aftershock sequence, a temporary strong-motion array was installed in the area where major damage took place. Some instruments were deployed on different geological and morphological soil conditions in two towns, Cesi and Sellano, to investigate the considerable localisation in the observed damage. Field investigations were also carried out to assess the geological profiles across strong-motion sites. The recordings confirmed the importance of site characteristics in the distribution of damage at sites very close to one another. Large amplification at the basin border of the Cesi site and an important three-dimensional effect at the site in Sellano were observed.

It has been demonstrated that the most important topographical parameter influencing local amplification of ground motion is the steepness of the ridge (Finn, 1991). Displacement amplifications at the crest of a triangular-shaped hill are equal to $2/\nu$, where ν is estimated

Table 1.8 Effects of topographic and subsurface irregularities.

Structure	Influencing factors	Effect	Quantitative	Predictability
Surface topography	Sensitive to shape ratio, largest for ratio between 0.2 and 0.6	Amplification at top of structure, rapid changes in amplitude phase along slopes	Ranges up to a factor of 30 but generally about 2–20	Poor: generally under-predict size; may be due to ridge-ridge interaction and three-dimensional effects
Shallow and wide (depth/width < 0.25) sediment-filled valleys	Effects most pronounced near edges; largely vertically propagating shear waves away from edges	Broadband amplification near edges due to generation of surface waves	One-dimensional models may under-predict at higher frequencies by about 2 near edges	Good: away from edges one dimension works well, near edges extend one dimension to higher frequencies
Deep and narrow (depth/width > 0.25) sediment-filled valleys	Effects throughout valley width	Broadband amplification across valley due to whole valley modes	One-dimensional models may under-predict for a wide bandwidth by about 2–4; resonant frequencies shifted from one-dimensional analysis	Fair: given detailed description of vertical and lateral changes in material properties

Adapted from Silva (1988).

from the angle formed by the ridges, that is π. Consequently, as the ridge becomes steeper the displacement amplification increases. Measured amplification at hill crests with respect to the base ranges between 2 and 20. The latter values are higher than those predicted analytically (generally between 2 and 4) because of the significant influence of both ridge-to-ridge interaction and three-dimensional effects, as, for example those observed in the town of Sellano during the 1997 Umbria-Marche (Italy) earthquake.

An exhaustive discussion of distance, travel path and site effects from seismological and geotechnical standpoints can be found in Reiter (1990) and Kramer (1996), respectively. Hereafter, directional effects, site amplification, dispersion and incoherence and their effects on structural response are outlined.

1.3.1 Directional Effects

Earthquakes of small magnitude are frequently generated by sources that may be represented by a point, since the fault rupture extends only a few kilometres. Conversely, for large earthquakes, fault rupture traces can be a few hundred kilometres long. In the latter case, seismic wave radiation is influenced by the source dimensions. Earthquake stress waves propagate in

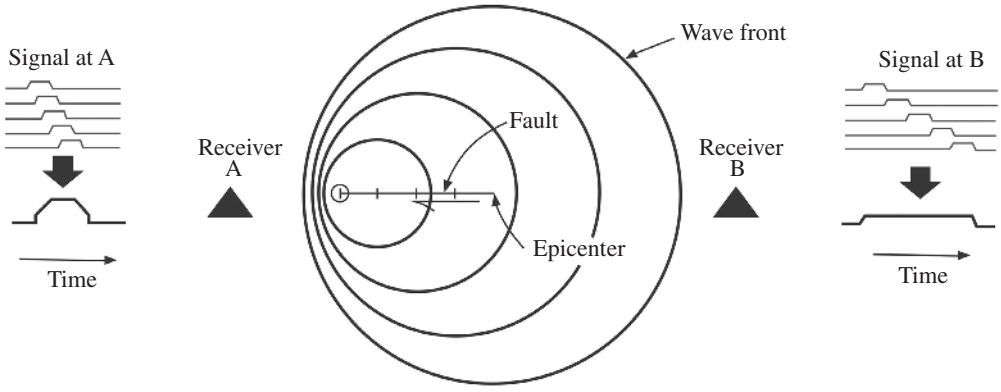

Figure 1.17 Directivity effects on sites towards and away from direction of fault rupture. (Adapted from Singh, 1985.)

the direction of faulting more intensely than in other directions. This affects the distribution of shaking intensity and hence the distribution of ground-motion parameters and consequently damage distribution. For example, waves propagate away from the fault rupture with different intensity along different directions; this observation is referred to as 'directivity'. Benioff (1955) and Ben-Menachem (1961) demonstrated that such directivity can lead to azimuthal differences in ground motions. Directivity occurs because fault ruptures are moving wave sources which travel at a finite velocity along the fault. The engineering implication of such directivity effects is that sites which are equidistant from the source will be subjected to varying degrees of shaking from the same earthquake, thus casting doubt over the concept of distance-based attenuation relationships discussed in Section 3.3. In Figure 1.17 a pictorial representation of directivity effects on ground motions at sites in the direction of, and away from, fault rupture is given. As the fault rupture (or earthquake source) moves away from the epicentre it generates ground motion from each segment of the breaking fault. The ground motion radiates outward in all directions and the seismic energy propagates through expanding wavefronts.

The overriding of stress waves or 'constructive interference' results in larger ground-motion magnification with shorter total duration in the direction of rupture propagation. Lower amplitude motions and longer total duration are exhibited in the opposite direction. This effect increases as the velocity of the fault rupture reaches the speed of seismic waves and as the angle between the point of observation (e.g. the recording station and construction site) and the direction of rupture propagation is reduced. Constructive interference, which is in essence a Doppler effect, generates strong pulses of large displacement or 'fling' at nearby sites towards which the fault rupture is progressing (Singh, 1985; Somerville *et al.*, 1997), for example towards the left in Figure 1.17. Rupture directivity also causes the polarisation of ground motion, that is differences between the fault-normal and fault-parallel components of horizontal ground-motion amplitudes (Stewart *et al.*, 2001). This polarisation causes more intense shaking in the fault-normal direction than in the fault-parallel direction. Where sufficient information exists, directivity effects should be taken into account in estimating earthquake design parameters. Directivity or focusing

of seismic energy caused severe damage to residential buildings and transportation systems in urban areas during the 1994 Northridge and 1995 Kobe earthquakes (Broderick *et al.*, 1994; AIJ, 1995). Damage to structures during past earthquakes is illustrated in detail in Appendix B.

1.3.2 Site Effects

The characteristics of the site affect the frequency and duration of earthquake ground motions. Structures founded on rock will, in general, be subjected to short-period (high-frequency) motion, while soft sites result in longer period (low-frequency) excitation. The ratio between the period of the site and that of the building is important in estimating the amplification effects; this is known as the 'site resonance effect'. Resonance is a frequency-dependent phenomenon. The site period T_S for uniform single soil layer on bedrock can be estimated from the relationship:

$$T_S = \frac{4H}{v_S} \tag{1.24.1}$$

where T_S is in seconds, H and v_S are the depth of soil layer (in metres) and soil shear wave velocity (in m/s), respectively. The shear wave velocity v_S of the soil layer is a function of the soil type and the depth of the deposit. The average values given in Table 1.9 may be used with Eq. (1.24.1); the latter equation provides the natural period of vibration of a single homogeneous soil layer. Periods associated with higher modes can be determined as follows:

$$T_{S,n} = \frac{1}{2n-1}\frac{4H}{v_S} \tag{1.24.2}$$

in which n represents the nth mode of vibration ($n > 1$).

Table 1.9 Shear wave velocities for foundation materials (in m/s).

Material (type)	Depth, H (in metres)		
	$1 < H < 6$	$7 < H < 15$	$H \geq 15$
Loose saturated sand	60	—	—
Sandy clay	100	250	—
Fine saturated sand	110	—	—
Clay/sand mix	140	—	—
Dense sand	160	—	—
Gravel with stone	180	—	—
Medium gravel	200	—	—
Clayey sand with gravel	—	330	—
Medium gravel	—	—	780
Hard sandstone	—	—	1200

In alluvial surface layers vibrations are amplified due to multi-reflection effects. The ratio of the amplitude a_g at the ground surface to the amplitude at the lower boundary layer (bedrock) a_b is given by (Okamoto, 1984):

$$\left|\frac{a_g}{a_b}\right| = \left(\cos^2\frac{\omega H}{v_s} + \alpha^2 \sin^2\frac{\omega H}{v_s}\right)^{-\frac{1}{2}} \tag{1.24.3}$$

in which ω is the natural circular frequency of the soil layer and α is the wave-propagation impedance given by:

$$\alpha = \frac{\rho_s v_s}{\rho_b v_b} \tag{1.24.4}$$

where ρ and v are the density and velocity of the surface layer (subscript s) and lower layer (subscript b), respectively.

The response of elastic layers of soil of finite depth H and varying shear rigidity G to earthquake ground motions was first investigated analytically by Ambraseys (1959). Auto-frequencies of the overburden were derived when the rigidity of the material G varies with depth. The latter is often encountered in practical applications in comparatively thin superficial weathered layers of soil or in desiccated soils in arid climates. Surface compaction may also produce a decrease in rigidity with depth. It was demonstrated that a good approximation of the periods of vibration can be obtained by considering the rigidity ratio k equal to the mean value $\bar{G}$ of shear modulus at the surface G and at the bedrock G_b and utilising the following relationship:

$$T_{S,n} = \frac{5.66}{2n-1}\frac{H}{v_S}\frac{k}{\sqrt{1+k^2}} \tag{1.25.1}$$

where n is the nth mode of vibration ($n > 1$), v_s the shear wave velocity near the surface of the layer of height H. The constant of rigidity is given by:

$$k = \sqrt{\frac{\bar{G}}{G_b}} \tag{1.25.2}$$

The expression in Eq. (1.25.1) holds within less than 6.0% of the true frequencies for small values of the rigidity ratio, that is $k \leq 1.5$–2.0. Alternatively, for layers of linearly increasing rigidity, the periods of layers of constant rigidity (as per Eqs. (1.24.1) and (1.24.2)) can be reduced through the factors provided in Table 1.10. Periods of vibrations of layers with uniform rigidity are always higher than those corresponding to a layer of linearly increasing rigidity. The listed correction factors are given for the first six modes of vibration and may be used to estimate site periods.

An example of significant site amplifications was observed in the 1985 Mexico City earthquake. On 19 September 1985 an earthquake of magnitude $M_S = 8.1$ struck the Mexican

Table 1.10 Reduction factors (in %) for period of elastic soil layers with uniform rigidity.

G_b/G	Mode (n)					
	1st	2nd	3rd	4th	5th	6th
1.00	0.0	0.0	0.0	0.0	0.0	0.0
1.10	3.4	2.5	2.4	2.3	2.1	2.0
1.21	6.6	5.0	4.9	4.6	4.6	4.6
1.32	9.5	7.5	7.1	7.0	6.9	6.9
1.56	15.0	11.7	11.3	11.1	11.1	11.0
1.96	22.0	17.2	17.0	16.7	16.6	16.6
2.25	28.7	20.8	20.3	20.0	20.0	20.0
4.00	41.7	34.6	34.0	33.6	33.5	33.4
9.00	59.1	51.6	50.6	50.4	50.2	50.1
25.00	74.6	68.5	67.3	67.1	66.8	66.8

After Ambraseys (1959).

capital and caused widespread structural damage especially downtown, as shown in damage pictures in Appendix B. More than 10 000 people were killed. Downtown Mexico City is built on sediments from an ancient 40-m-thick soft layer of lake deposits. The average shear wave velocity of the soil layer is about 80 m/s and hence the resonant period T_S computed from Eqs. (1.24.1) and (1.24.2) is about 2.0 seconds (0.5 Hz). Medium-to-high rise buildings with 5-to-15 storeys were particularly susceptible to damage (e.g. Osteraas and Krawinkler, 1990). These structures exhibit fundamental periods close to the resonant value T_S. Site amplifications also caused several structural collapses during the 1994 Northridge earthquake, in California (Broderick *et al.*, 1994).

It is recommended that the ratio between the building and site periods be as distinct from unity as possible. In estimating the period of the site, assessment of the deep geology, not only the surface soil condition, is crucial. Higher vibration modes of the site should be checked with respect to the predominant response periods of the structure under consideration.

The nature of soil response in earthquakes depends on the amplitude and duration of motion. High-amplitude motion tends to cause inelasticity in the soil. Long-duration shaking increases the susceptibility to liquefaction of saturated and partially saturated soils. When the soil responds elastically, the observed motions at the surface are amplified proportional to the input ground motion. On the other hand, for inelastic response, the soil absorbs large amounts of the energy corresponding to large amplitude of ground motions. Therefore, in general, large earthquake vibrations travelling through inelastic media will exhibit lower accelerations (relative to small magnitude earthquakes) and large displacements, corresponding to long periods. The displacement demand on structural systems is thus increased, especially on medium- and long-period structures, such as high-rise multistorey buildings and long-span bridges. Long-duration shaking applies a large number of cycles that may cause a significant increase in pore water pressure leading to total loss of cohesion in soils that then turn into a liquid. This is referred to as liquefaction (e.g. Kramer, 1996, among others).

1.3.3 Dispersion and Incoherence

Earthquake ground motion may exhibit spatial variability on regional and local levels. Large-scale effects are described mathematically by attenuation relationships which are presented in Section 3.3. Herein, two strong-motion characteristics associated with local spatial variations, that is 'dispersion' and 'incoherence', are discussed primarily from a physical, as opposed to a mathematical, point of view.

Dispersion and incoherence may be caused by several factors. They can be thought of as the result of the combination of three basic effects as shown in Figure 1.18 and summarised below (Abrahamson, 1991):

(i) *Wave passage effect:* represents the time delay in the arrival of seismic waves on the ground surface at different stations or sites. This effect is due to the finite travelling velocity of seismic waves through media (see Section 1.1.3).
(ii) *Extended source effect:* number and size of earthquake sources affecting the seismicity at a site may cause delays in the arrival time of waves. This time lag generates different motions at different points.
(iii) *Ray path effect (or scattering effect):* caused by reflection and refraction of waves through the soil during their propagation, inhomogeneities of soil layers and other differences in local soil conditions under the various stations.

Spatial variability of earthquakes can be described mathematically either in the time domain (generally by auto-covariance and cross-covariance) or frequency domain (by coherency functions). It is beyond the scope of this chapter to discuss analytical techniques employed to define dispersion and incoherence. The reader may consult one of the textbooks which deal specifically with random vibrations in earthquake engineering (e.g. Manolis and Koliopoulos, 2001, among others). It is noteworthy that ground motions recorded by dense arrays in several regions worldwide, for example USA, Japan and Taiwan, have shown coherency decreases with increasing distance between measuring points and increasing frequency of motion (e.g. Clough and Penzien, 1993; Kramer, 1996). The coherency of two ground motions is a measure of correlation of amplitudes and phase angles at different frequencies. Incoherence (or loss of coherence) is strongly frequency-dependent (Luco and Wong, 1986). The coherence factor or absolute value of coherency is a measure of the incoherence. More significant effects are observed at higher frequencies: for frequencies lower than 1.0–2.0 Hz (periods T of 0.5–1.0 seconds) the loss of coherence can be ignored (coherence factor is close to 1.0). Coherence

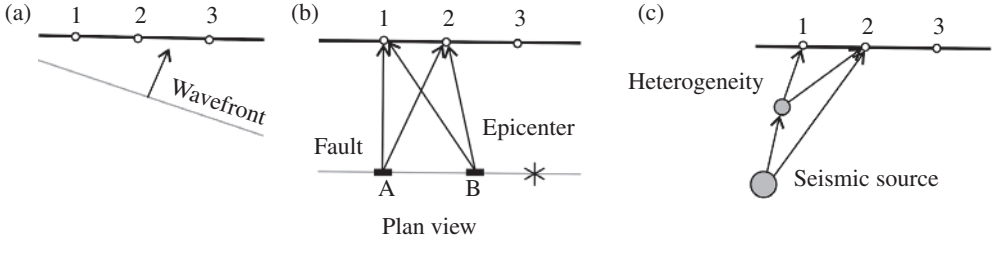

Figure 1.18 Sources of local spatial variability of ground motions: wave passage effect (a), extended source effect (b) and ray path effects (c).

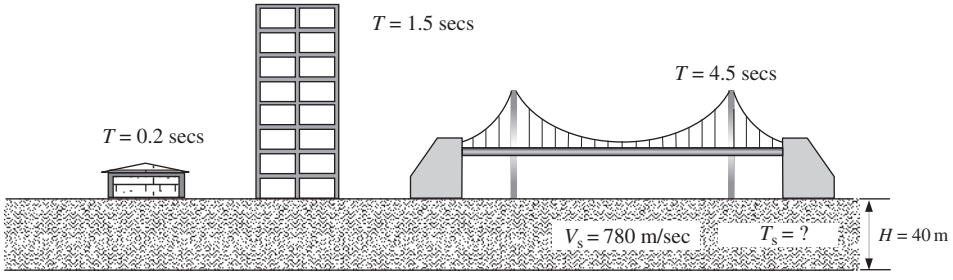

Figure 1.19 Structural systems with different natural periods of vibration.

starts to decrease significantly for higher frequencies. For frequencies higher than 5 Hz (T less than 0.2 seconds) the coherence factor is reduced by more than 40–50%. Several expressions for smooth coherence functions have been proposed for design purposes (e.g. Luco and Wong, 1986; Haricharan and Vanmarcke, 1986; Abrahamson, 1991; Oliveira *et al*., 1991 Somerville *et al.*, 1991; Der Kiureghian, 1996). These relationships typically depend on the separation distance and frequency.

Dispersion and incoherence of earthquake ground motions do not generally affect short-span structures, such as buildings, but they may significantly influence the dynamic response of long-span structures, for example medium- to long-span bridges, stadiums and pipelines that extend over considerable distances. Significant spatial variability may often occur whenever the large plan dimensions are combined with irregularities in the soil profile along the travel path. For long distances and rather stiff structures totally uncorrelated ground motions with appropriate frequency content should be considered. Loss of coherence can be ignored in all the other cases, although time delay should always be accounted for.

Problem 1.4

What is the natural period of a layered soil with medium gravel of depth 40 m? Is it safe to build a multi-storey framed building with fundamental period of vibration equal to 1.5 seconds, as that displayed in Figure 1.19, on a site with the above soil type? Is this site more suitable for a particular type of structure shown in Figure 1.19?

1.4 Effects of Earthquakes

Comprehensive regional earthquake impact assessment requires an interdisciplinary framework that encompasses the definition of the hazard event, physical damage and social and economic consequences. Such an integrated framework may provide the most credible estimates with associated uncertainty that can stand scientific and political scrutiny. Physical damage should be evaluated for the building stocks, lifeline systems, transportation networks and critical facilities. Short- and long-term effects should be considered in quantifying social and economic consequences. Figure 1.20 provides an overview of causes and effects of natural disasters.

The fundamental components of earthquake loss assessment are (i) hazard, (ii) inventory and (iii) vulnerability or fragility, as depicted in Figure 1.21. Seismic risk is the product of

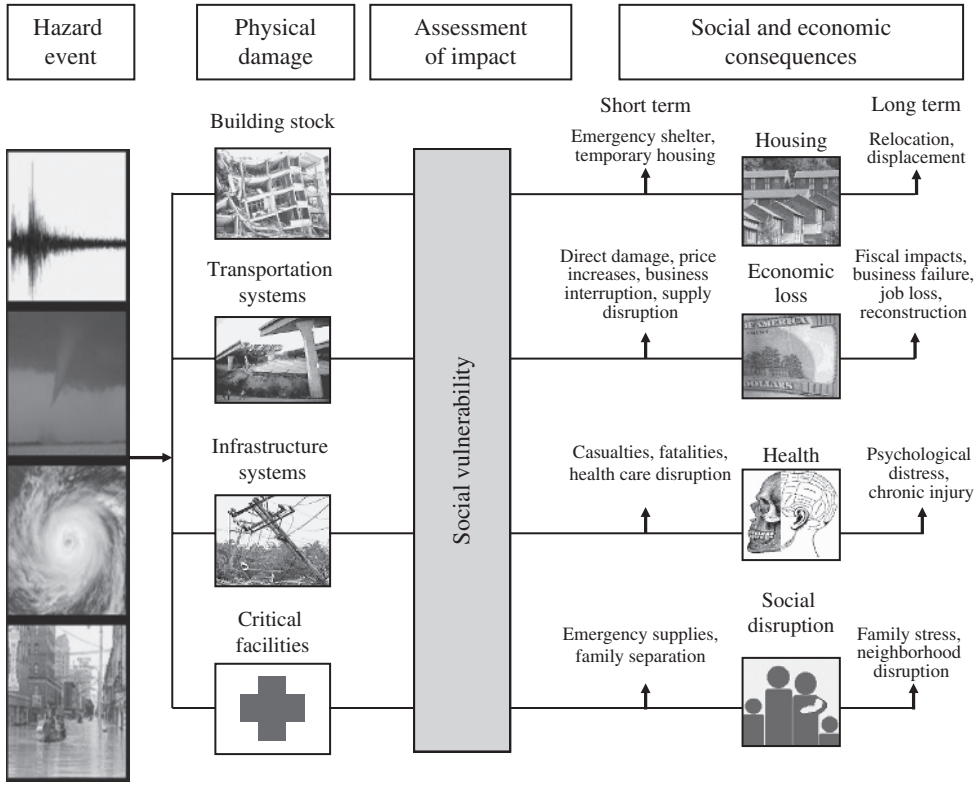

Figure 1.20 Correlation between typical hazard events and social and economic consequences. (Courtesy of Steve French.)

hazard and vulnerability for a unit value of assets. Hazard or exposure is the description of the earthquake ground motion. In this book, the hazard is described in general in this opening chapter while detailed characterisation of the earthquake input motion is given in Chapter 3. Inventory comprises the assets that are subjected to the hazard; thus, it is a count of the exposed systems and their value. Inventory issues and technologies are beyond the scope of this book. Vulnerability or fragility is the sensitivity of the assets to damage from intensity of ground shaking. The vulnerability of structural systems is addressed conceptually in Chapter 2 and in a detailed manner in Chapters 4 and 5. From an earthquake engineer's perspective, hazard can be quantified but not reduced. Vulnerability can be both evaluated and reduced, by measures of retrofitting for example. Vulnerability can also be reduced by other means, such as long-term land-use management and education. Obtaining accurate inventories of exposed assets and their values remains a significant challenge that requires not only technical tools, but also political will and national commitment, especially in regions where private industry holds large inventory data sets that are not in the public domain.

Earthquakes can cause devastating effects in terms of loss of life and livelihood. The destructive potential of earthquakes depends on many factors. The size of an event (expressed by either intensity or magnitude as described in Sections 1.2.1 and 1.2.2), focal depth and

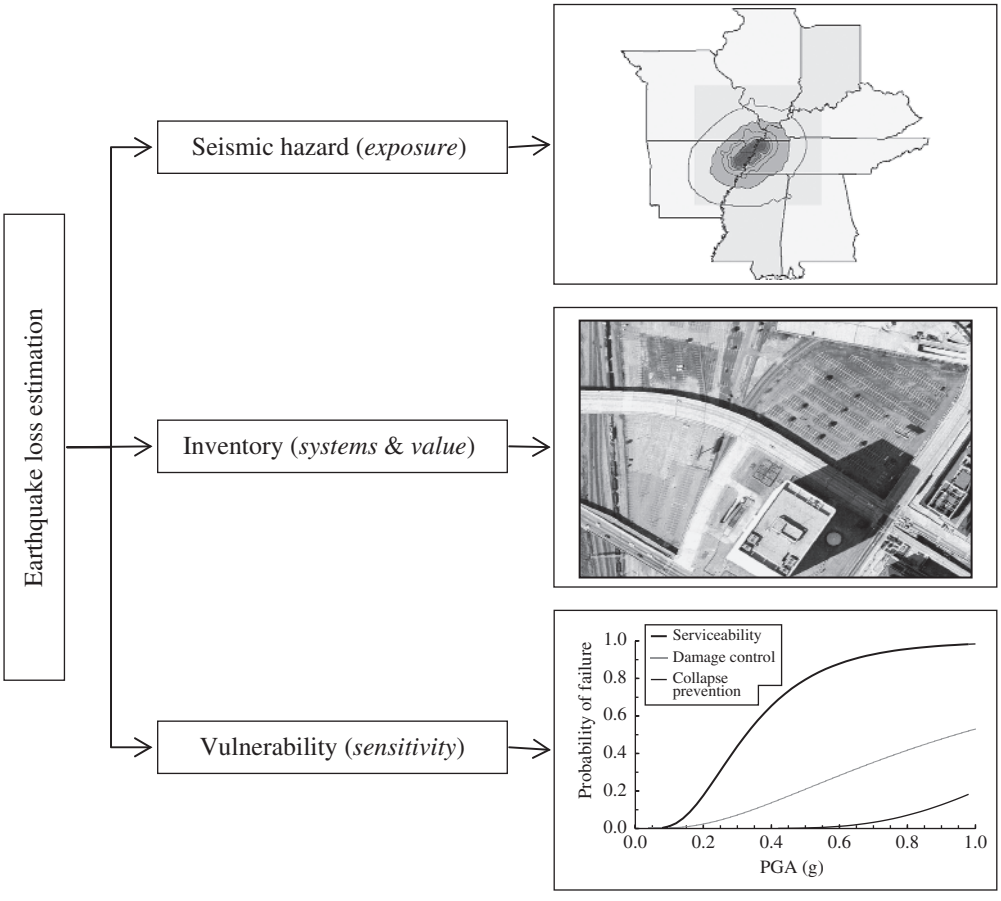

Figure 1.21 Basic components for earthquake loss estimations.

epicentral distance, topographical conditions and local geology are important earthquake characteristics. However, the causes of fatalities and extent of damage depend to a great extent on the type of constructions and the density of population present in the area. Earthquakes exact a heavy toll on all aspects of exposed societal systems. They can have several direct and indirect effects as shown in Figure 1.22.

Ground shaking is by far the most important hazard resulting from earthquakes, with some exceptions (e.g. the Asian tsunami of 26 December 2004 with about 280 000 people killed). Structural damage, which is a feature of the primary vertical and lateral load-resisting systems, may vary between light damage and collapse. Non-structural damage consists of the failure or malfunctioning of architectural, mechanical and electrical systems and components within a building. Non-structural damage may lead to large financial losses as well as pose significant risk to life. Further details on non-structural damage can be found, for example in ATC (1998) and the reconnaissance reports published in the aftermath of damaging earthquakes.

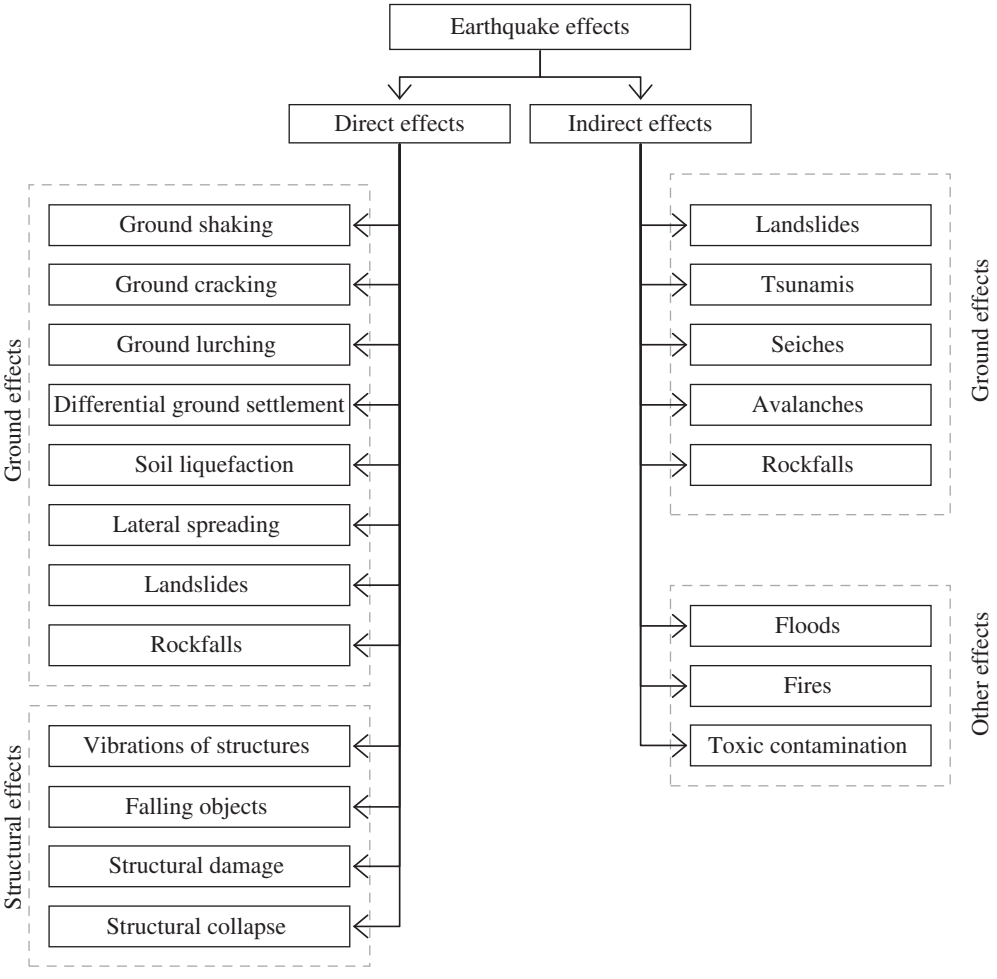

Figure 1.22 Direct and indirect earthquake effects.

1.4.1 Damage to Buildings and Lifelines

Extensive structural damage is suffered by buildings, bridges, highways and other lifelines during earthquakes. Seismic vulnerability of structures varies as a function of construction materials and earthquake action-resisting system employed. Typical damage to masonry, reinforced concrete (RC), steel and composite (steel–concrete) buildings is summarised in Table 1.11. Damage is classified under the categories of structural members, connections and systems. It should be noted that in some cases a pattern of damage is common to different structural members. For example, shear failure may occur in RC beams and columns. Moreover, local buckling may affect steel beams, columns and braces. Several examples of damage to buildings and bridges are provided in Appendix B, which also contains a detailed discussion of common structural deficiencies observed for steel, concrete

Table 1.11 Typical damage to building structures.

Masonry and RC		Steel and composite	
Structural element/system	Observed damage	Structural element/system	Observed damage
Beams	Shear failure, concrete cover spalling, reinforcing bar buckling	Beams	Flange and web yielding, local buckling, brittle fracture
Columns	Cracking, crushing, concrete cover spalling, reinforcing bar buckling and pull-out, flexural and shear failure, short column effect	Columns	Flange yielding, local buckling, brittle fracture, splice failure, member buckling
Connections	Cracking, crushing, reinforcing bar buckling and pull-out, shear failure	Braces	Local and member buckling, brittle fracture
Structural walls and infills	X-shaped cracks, crushing, reinforcing bar buckling, overturning, rocking, sliding	Connections	Yielding, local buckling, brittle fracture, weld cracks, excessive panel deformations, bolt rupture
Foundations	Settlement, reinforcing bar pull-out, rocking, sliding, uplifting	Foundations	Bolt anchorage rupture, weld cracks and fracture, pull-out, excessive base plate deformations
Frames	Soft and weak storeys, excessive residual deformations, distress in diaphragms and connectors, pounding, rocking, uplifting, fall of parapets and brick chimneys	Frames	Soft and weak storeys, excessive residual deformations, distress in diaphragms and connectors, pounding, uplifting

and masonry systems. Timber structures have been used extensively especially in Japan, New Zealand and the USA. They include both older non-engineered single-storey family residences and newer two-to-three storey apartment and condominium buildings. Wood-framed buildings are inherently lightweight and flexible; both features are advantageous under earthquake loading conditions (Ambrose and Vergun, 1999). Low-to-medium rise wood buildings, however, have been affected by structural damage during large earthquakes (Bertero, 2000). Observed damage consists of cracking in interior walls and brick chimneys, cracking and collapse of brick veneer on exterior walls. Wooden constructions have often experienced failures similar to those of masonry buildings. Indeed, several partial or total collapses are due to soft and weak storeys, insufficient lateral bracing and inadequate ties and connections between the components of the building. Inadequate foundation anchorage led to uplifting and sliding in many cases during recent earthquakes in California (e.g. Baker *et al*., 1989; Andreason and Rose, 1994, among others).

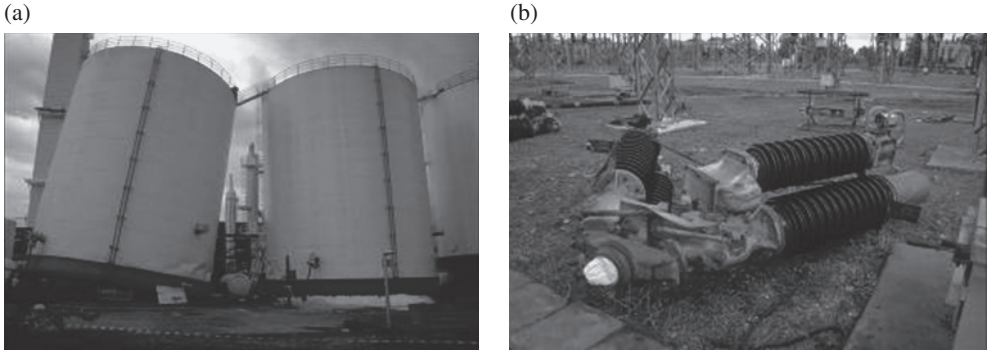

Figure 1.23 Tilting of oxygen tanks (a) and brittle fracture of circuit breaker (b) during the 1999 Izmit (Turkey) earthquake. (Courtesy of A.S. Whittaker.)

Lifelines are those services that are vital to the health and safety of communities and the functioning of urban and industrial regions. These include electric power, gas, water and wastewater systems. Infrastructures, such as transportation systems (highways and railways), bridges, ports and airports are also classified as lifelines. Damage to lifelines imposes devastating economic effects on the community. Their seismic performance affects emergency response, short-term and long-term recovery. Broken gas and power lines are serious threats to safety, largely because of risk of fire and explosions. The lack of water also inhibits fire-fighting efforts. Leaks and rupture of wastewater systems may lead to toxic contamination. For example, during the 1995 Kobe earthquake, the destruction of lifelines and utilities made it impossible for fire-fighters to reach fires started by broken gas lines (Bukowski and Scawthorn, 1995; Elnashai *et al.*, 1995; Scawthorn *et al*., 2005). Large sections of the city burned, greatly contributing to the loss of life. Examples of damage to fuel tanks and electrical power systems are displayed in Figure 1.23. Tilting and 'elephant foot' buckling are common failure modes of fluid-holding steel tanks, while brittle fractures are generally observed in substations, which receive and distribute energy to large urban areas. The major causes of outages during past earthquakes were the catastrophic failures of circuit breakers, transformer bushings and disconnected switches at substations. Major damage to lifelines observed during recent earthquakes is summarised in Table 1.12.

The list of types of damage in Table 1.12 is indicative rather than exhaustive, given the variety and complexity of lifeline systems, which are beyond the scope of this book. Several textbooks and manuals that specialise in this subject are available (e.g. Okamoto, 1984; Taylor *et al*., 1998 and VanMarcke, 2002; among others). Reconnaissance reports of damage to lifelines are published by the Earthquake Engineering Research Institute on the Internet (http:\\www.eeri.org).

1.4.2 Effects on the Ground

Analysis of earthquake-induced damage indicates that ground effects are a serious contributor to damage of the built environment. Local geology and topography influence the travel path

Table 1.12 Typical damage to lifelines.

Highways and railways	Gas and electric power	Water and waste systems	Communication systems
Bending and shear failure of RC piers	Cracks and ruptures in the network	Breakage of pipelines and leakages in the network	Damage to electronic switching systems
Local and overall buckling of steel and composite piers. Brittle fracture of welded components	Brittle fracture to porcelain components in high-voltage transmission stations and substations	Sloshing and suction damage in metal storage tanks	Damage to phone lines
Pounding and unseating at hinge seats and deck supports	Damage to switching systems, cranes and tanks in power plants	Elephant foot and shell buckling in metal tanks	Damage to telephone system buildings
Cracks, large gaps and settlements in pavements of highways	Disruptions of electric power supply	Cracks and leaks in concrete basins	Malfunctioning of computer networks
Rails bending or rupture and train derails	Fires and explosions due to gas leaks	Malfunctioning of process equipments associated with ground settlement or rocking	Malfunctioning and collapse of transmission towers

and amplification characteristics of seismic waves. For example, natural and artificial unconsolidated foundation materials, such as sediments in river deltas and materials used as landfill, amplify ground motions in comparison to motion measured on consolidated sediments or bedrock. The thickness of unconsolidated soil also affects the ground shaking, as discussed in Section 1.3.2. Quasi-resonance between the underlying soil layers and the structures has led to increased damage during past earthquakes as presented in preceding sections of this book. Ground motions may be amplified by sedimentary layers with various thicknesses and degrees of consolidation.

In addition to direct shaking effects, earthquakes may lead to several forms of ground failure which cause damage to the built environment. For example, the more than $200 million in property losses and a substantial number of deaths in the 1964 Alaska earthquake (M_S = 8.6) were due to earthquake-induced ground failures. Similarly, soil effects were clear in the 1971 San Fernando and the 1989 Loma Prieta earthquakes in California. In particular, many apartment buildings in the Marina District of San Francisco suffered damage because of soil liquefaction. Geological and geotechnical aspects of earthquakes are beyond the scope of this book. A detailed treatment of geotechnical earthquake engineering may be found in Kramer (1996). Failure modes that are of primary concern for structural earthquake engineering are summarised below. Effects of water waves, such as tsunamis (or sea waves) and seiches (or lake waves), are not discussed hereafter. Readers can consult the available literature (e.g. Steinbrugge, 1982; Kanai, 1983; Okamoto, 1984; Bolt, 1999).

1.4.2.1 Surface Rupture

Rupture of the ground surface may be induced by intense and long shaking as well as fault ruptures. These may generate deep cracks and large gaps (ranging in size from a few metres to several kilometres). Damage by fault rupture is more localised than the widespread damage caused by ground shaking. Nine kilometres of surface rupture along the Nojima fault on Awaji Island was observed in the 1995 earthquake in Japan (Figure 1.24). From left to right along the rupture shown in Figure 1.24, an earthquake-induced landslide covers a road, a fault scarp across a rice paddy and a right-lateral offset in a dirt road. The section of rice paddy to the right has been uplifted by more than 1 m; light damage was experienced by buildings even at very close distances to the fault.

The effects of major fault ruptures can be extreme on structures; buildings can be ripped apart. Cracks and gaps in the ground may also cause serious damage to transportation systems (highways, railways, ports and airports) and underground networks (water, wastewater and gas pipes, electric and telephone cables). Earthquake-induced ground shaking may cause cracking of the ground surface in soft, saturated soil (defined as 'lurching' or 'lurch cracking'). Movements of soil or rock masses at right angles to cliffs and steep slopes occur. Structures founded either in part or whole on such masses may experience significant lateral and vertical deformations.

1.4.2.2 Settlement and Uplift

Fault ruptures may cause large vertical movements of the ground. These movements in turn cause severe damage to the foundations of buildings, bridge footings and to underground networks. The collapse of several approach structures and abutments of bridges was observed in the San Fernando (1971), Loma Prieta (1989), Northridge (1994) and Kobe (1995) earthquakes. Settlement, tilting and sinking of buildings have been observed in the aftermath of several earthquakes worldwide. Differential ground settlements may cause structural distress. Granular soils are compacted by the ground shaking induced by earthquakes, leading to subsidence. This type of ground movement affects dry, partially saturated and saturated soils with high permeability. Subsidence of 6–7 m

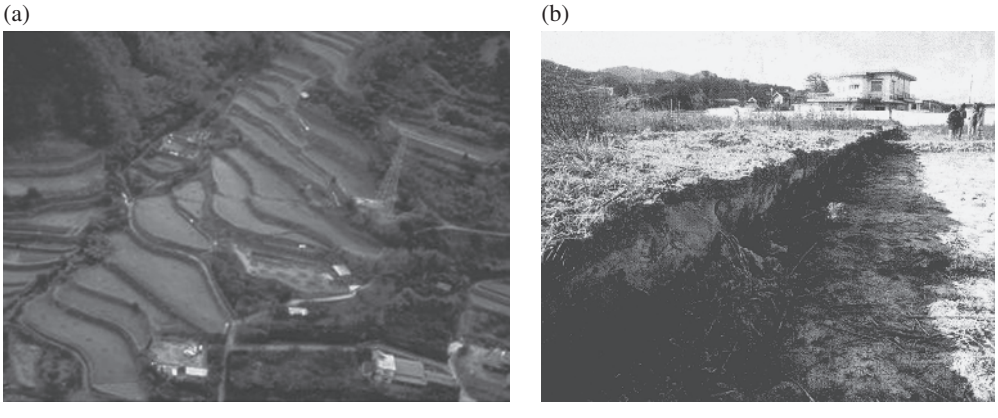

Figure 1.24 Fault rupture observed on northern Awaji Island during the 1995 Kobe (Japan) earthquake: aerial view with the fault rupture that cuts across the middle of the picture (a) and close-up showing both vertical and horizontal offset of the Nojima fault (b).

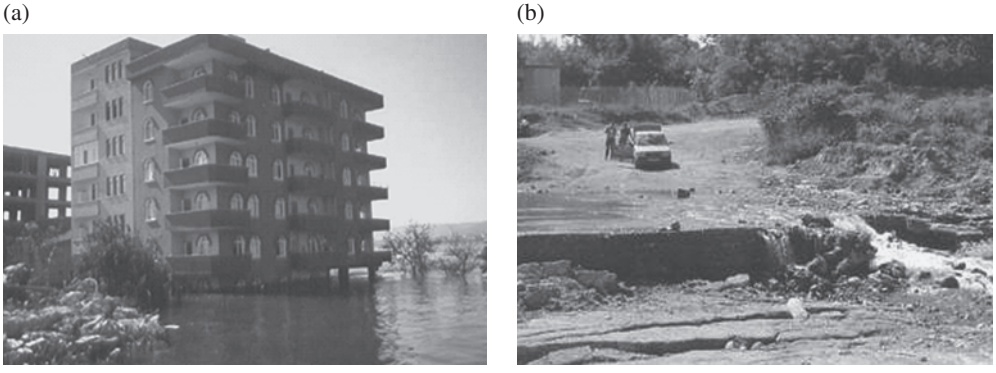

Figure 1.25 Effects of ground settlements and uplift during the 1999 Kocaeli (Turkey) earthquake: flooding (a) and artificial water falls (b).

was observed during the New Madrid earthquakes (1811–1812) in the Mississippi Valley in the USA. Subsidence of areas close to sea, lakes and river banks may cause flooding of ports, streets and buildings. In some cases artificial water falls may also be generated by settlements and uplifts as shown in Figure 1.25, from the Kocaeli, Turkey, earthquake of 1999.

1.4.2.3 Liquefaction

Excessive build-up of pore water pressure during earthquakes may lead to the loss of stiffness and strength of soils. The excessive pore water pressure causes ejection of the soil through holes in the ground, thus creating sand boils. Figure 1.26 shows two examples of liquefaction during the 1998 Adana–Ceyhan (Turkey) and the 2001 Bhuj (India) earthquakes. The ejection of soil causes loss of support of foundations and thus structures tilt or sink into the ground. Massive liquefaction-induced damage has been observed in the two Niigata earthquakes of 1964 and 2004 as well as the recent Pisco-Chincha (Peru) earthquake of 2007, as discussed below.

Retaining walls may tilt or break from the fluid pressure of the liquefied zone. Heavy building structures may tilt due to the loss of bearing strength of the underlying soil. During the 1964 Niigata, Japan, earthquake (M_S = 7.5), four-storey apartment buildings tilted 60° on liquefied soils as shown in Figure 1.27. Similarly, in the 1989 Loma Prieta earthquake, liquefaction of the soils and debris used to fill in a lagoon caused major subsidence, fracturing and horizontal sliding of the ground surface in the Marina district in San Francisco.

Soil liquefaction may cause the floating to ground surface of pile foundations with low axial loads and underground light-weight storage tanks. In Kobe lateral spreading damaged the pile foundations of several buildings and bridges (Figure 1.27) because of horizontal movements. Quay walls and sea defences in the port of Kobe were also affected by soil liquefaction.

1.4.2.4 Landslides

Landslides include several types of ground failure and movement, such as rockfalls, deep failure of slopes and shallow debris flows. These failures are generated by the loss of shear strength in the soil. Landslides triggered by earthquakes sometimes cause more destruction

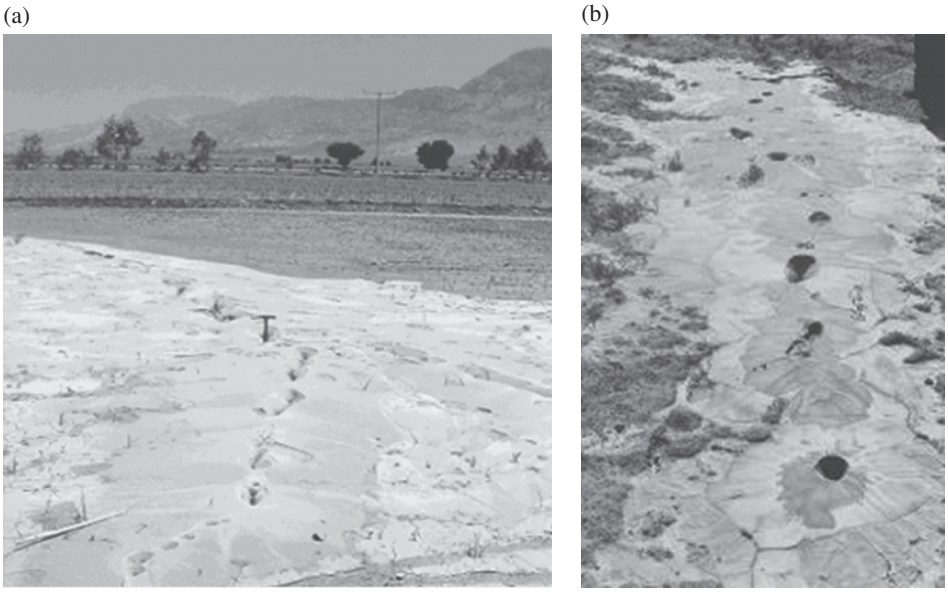

Figure 1.26 Sand boils due to the 1998 Adana–Ceyhan (Turkey) earthquake (a) and the 2001 Bhuj (India) earthquake (b).

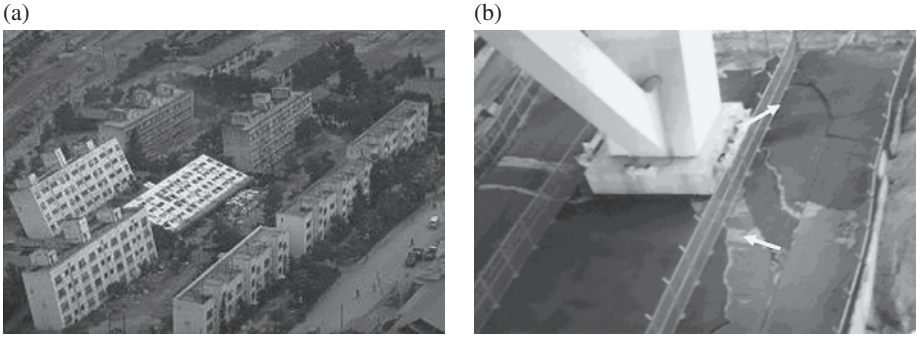

Figure 1.27 Collapses due to soil liquefaction: settlement and tilting of buildings in the 1964 Niigata (Japan) earthquake (a); soil boils and cracks at pier foundations of Nishinomiya-ko bridge in the 1995 Kobe (Japan) earthquake (b). (After NISEE.)

than the earthquakes themselves. Immediate dangers from landslides are the destruction of buildings on or in the vicinity of the slopes with possible fatalities as rocks, mud and water slide downhill or downstream. Electrical, water, gas and sewage lines may be broken by landslides. The size of the area affected by earthquake-induced landslides depends on the magnitude of the earthquake, its focal depth, the topography and geologic conditions near the causative fault and the amplitude, frequency content and duration of ground shaking. During the 1964 Alaska earthquake, shock-induced landslides devastated the Turnagain Heights residential development and many downtown areas in Anchorage. One of the most spectacular

Figure 1.28 Effects of a large landslide in Santa Monica in the 1994 Northridge earthquake (a) and satellite view of extensive land-sliding during the 2005 Kashmir earthquake in the Neela Dandi Mountain (b).

landslides observed, involving about 9.6 million m^3 of soil, took place in the Anchorage area. The scale of such landslides on natural slopes can be large enough to devastate entire villages or towns, such as the Huascaran Avalanche triggered by the Peru earthquake (1970, $M_w = 7.8$). Most of the more than 1000 landslides and rockfalls occurred in the epicentral zone in the Santa Cruz Mountains during the 1989 Loma Prieta earthquake. One slide, on State Highway 17, disrupted traffic for about 1 month. In the 1994 Northridge earthquake, landslides that occurred in Santa Monica, along the Pacific Coast Highway, caused damage to several family houses built on the cliffs overlooking the ocean. This is shown in Figure 1.28. Relatively few landslides were triggered by the Hyogo-ken Nanbu earthquake in Japan. This is partly due to the fact that the earthquake occurred during the dry season. Landslides are often triggered by rainfall pressure generated inside fractured ground.

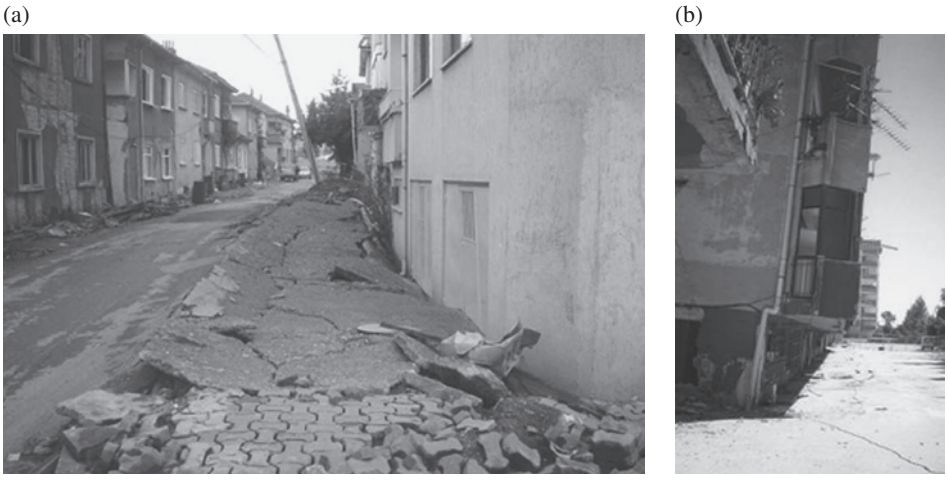

Figure 1.29 Damage observed during the 17 August 1999 Kocaeli in Adapazari (a) and Izmit in Turkey (b).

In the Kashmir earthquake of 8 October 2005, land-sliding and critical slope stability was a multi-scale problem that ranged from limited sloughing of a superficial nature to a scale that encompassed entire mountain sides (Durrani *et al.*, 2005). The land-sliding problem in the mountains of Azad Jammu and Kashmir and North West Frontier Province, Pakistan has similarities to land-sliding that occurred in the mountains of Central Taiwan due to the 1999 Chi-Chi earthquake. Figure 1.28 shows a large-scale landslide in the Neela Dandi Mountain to the north of Muzaffarabad. The satellite image shows that the landslide blocked the Jhelum River.

Problem 1.5

The 17 August 1999 Kocaeli (M_w = 7.4) and 12 November 1999 Düzce (M_w = 7.2) earthquakes were the largest natural disasters of the twentieth century in Turkey after the 1939 Erzincan earthquake. These earthquakes caused severe damage and collapse especially of building structures. Figure 1.29 shows damage observed in the cities of Adapazari and Izmit (Kocaeli earthquake). Comment on the relationship between the observed damage and the earthquake-induced ground effects illustrated in Section 1.4.2.

1.4.3 Human and Financial Losses

During the twentieth century over 1200 destructive earthquakes occurred worldwide and caused damage estimated at more than $1 trillion (Coburn and Spence, 2002). If these costs are averaged over the century, annual losses are about $10 billion. Monetary losses from earthquakes are increasing rapidly. Between 1990 and 1999 annual loss rates were estimated at $20 billion, twice the average twentieth-century annual losses. The Federal Emergency Management Agency released a study (FEMA, 2001) estimating annualised earthquake losses to the national building stocks in the USA at $4.4 billion, with California, Oregon and Washington accounting for $3.3 billion of the total estimated amount. An update of the above

landmark study was released in 2006 (www.fema.gov) to include in the estimation of the annualised losses three additional features of earthquake risk analysis, that is casualties, debris and shelter. In the latter study it is estimated that the annualised earthquake losses to the national building stock are $5.3 billion and about 65% is concentrated in the State of California. The largest earthquake in modern times in the USA was the 1964 Alaska earthquake, measuring 8.4 on the Richter scale. The earthquake caused $311 million in damage and 115 fatalities. In a historical context, the largest recorded earthquakes in the contiguous USA are the New Madrid earthquakes of 1811 and 1812. In the USA, 39 out of 50 states (nearly 80%) are at risk from damaging earthquakes. The Central and Eastern States in the USA now recognise earthquakes as a major threat. In particular the eight central States of Illinois, Arkansas, Indiana, Tennessee, Kentucky, Mississippi, Alabama and Missouri have dedicated considerable resources to work with FEMA and other earthquake engineering organisations to assess the possible impact of earthquakes and to mitigate as well as plan for response and recovery from their effects.

With regard to loss of life on average 10 000 people per year were killed by earthquakes between 1900 and 1999 (Bolt, 1999). In 2001 three major earthquakes in Bhuj (India, $M_S = 7.9$), El Salvador ($M_S = 7.6$) and Arequipa (Peru, $M_S = 8.4$) caused more than 26 000 casualties. The Bam (Iran, $M_S = 6.6$) and Sumatra (Indian Ocean, $M_W = 9.3$) earthquakes, which occurred in 2003 and 2004, both on 26 December, caused more than 26 000 and 280 000 deaths, respectively. The Kashmir earthquake of 8 October 2005 caused over 85 000 deaths. The human death toll due to earthquakes between 1900 and 2007 is given in Figure 1.30 (www.usgs.gov). Over this 108-year period, deaths due to earthquakes totalled about 1.8 million. China accounted for more than 30% of all fatalities.

Figure 1.31 compares the human death toll due to earthquakes with that caused by other natural hazards (www.usgs.gov). It is observed from the figure that earthquakes rank second after floods; earthquakes account for about 3.6 million fatalities. If the death toll caused by tsunamis is added to that caused by earthquakes, the total figure would amount to around 4.5 million.

Monetary losses due to collapsed buildings and lifeline damage are substantial. Furthermore, the economic impact of earthquakes is increasing due to the expansion of urban development and the higher cost of construction. For example, the 1994 Northridge earthquake, which is said to be the most costly natural disaster in the history of the USA, caused $30 billion in damage and $800 billion replacement value on taxable property (Goltz, 1994). In this event 25 000 dwellings were declared uninhabitable, while buildings with severe and moderate damage numbered 7000 and 22 000, respectively. Unexpected brittle fractures were detected in more than 100 steel-framed buildings as illustrated in Appendix B. Damage to the transportation system was estimated at $1.8 billion and property loss at $6.0 billion. In the above-mentioned earthquake the most severe damage occurred to non-retrofitted structures, designed in compliance with seismic regulations issued in the 1970s.

Several reconnaissance reports have concluded that building collapses caused 75% of earthquake fatalities during the last century. Other major causes of death were fires and gas explosions, tsunamis, rockfalls and landslides. In the Loma Prieta earthquake, 42 out 63 deaths (about 63%) were attributed to bridge failures. However, in the 1995 Kobe earthquake in Japan, 73% of the deaths were caused by collapsed houses. The likelihood of the collapse of multi-storey RC structures in developing countries, where the quality of construction remains relatively substandard, is high.

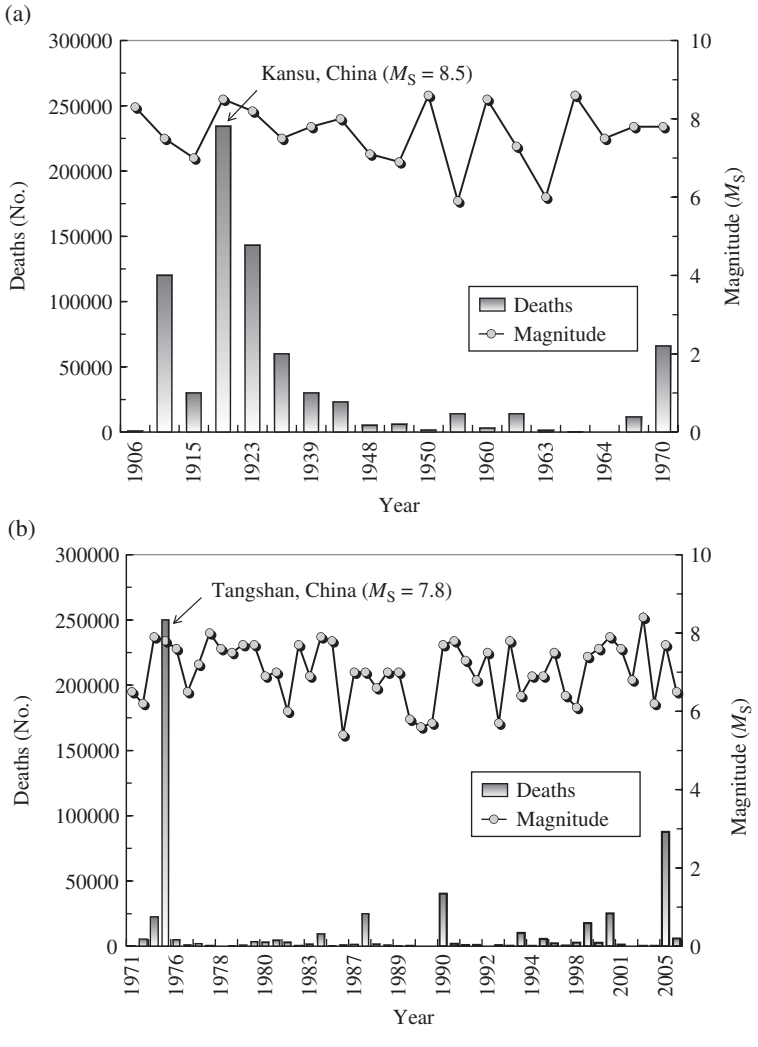

Figure 1.30 Human death toll due to earthquakes: 1900–1970 (a) and 1971–2007 (b).

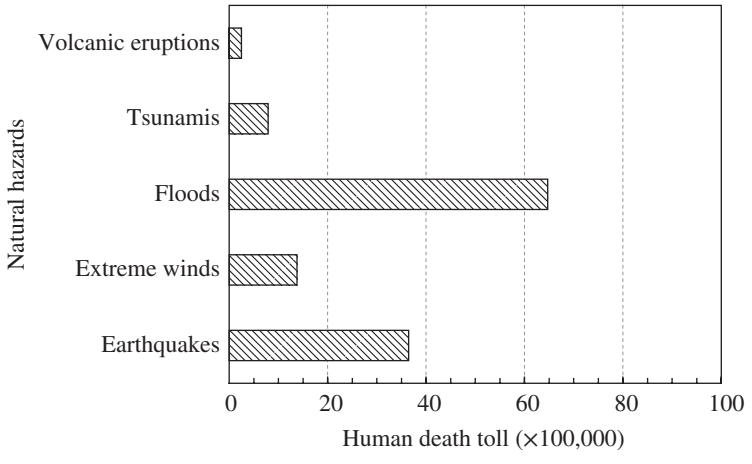

Figure 1.31 Human death toll caused by major natural hazards.

Table 1.13 Earthquake financial losses.

Country	Earthquake	Year	Loss ($ bn)	GNP ($ bn)	Loss (% GNP)
Nicaragua	Managua	1972	2.0	5.0	40.0
Guatemala	Guatemala City	1976	1.1	6.1	18.0
Romania	Bucharest	1977	0.8	26.7	3.0
Yugoslavia	Montenegro	1979	2.2	22.0	10.0
Italy	Campania	1980	45.0	661.8	6.8
Mexico	Mexico city	1985	5.0	166.7	3.0
Greece	Kalamata	1986	0.8	40.0	2.0
El Salvador	San Salvador	1986	1.5	4.8	31.0
USSR	Armenia	1988	17.0	566.7	3.0
Iran	Manjil	1990	7.2	100.0	7.2

GNP = Gross national product.
After Coburn and Spence (2002).

Earthquake damage resulting in the collapse of monuments, historical places of worship and stately buildings represents an irreplaceable loss in terms of cultural heritage, while their restoration costs exceed by far the GNP of many affected nations. The expense of reconstructing the world-famous vault of the Basilica at Assisi (Italy) with its early Renaissance frescoes caused serious repercussions for the national economy after 1997. Even more problematic are the implications for important heritage sites in seismically active developing countries. The earthquakes of Gujarat (India), Bam (Iran), Arequipa (Peru) and Yogyakarta (Indonesia) have caused major damage to invaluable historical sites that may or may not be restored over a number of years and at an extremely high cost.

One of the most severe consequences of earthquakes is the cost of recovery and reconstruction. It is instructive to note, however, that the absolute financial loss is less critical to an economy than the loss as a percentage of the GNP. For example, in some 6 to 8 seconds, Nicaragua lost 40% of its GNP due to the 1972 Managua earthquake (Table 1.13), while the 800% higher bill ($17 billion versus $2 billion) from the 1988 Yerevan, Armenia earthquake constituted only 3% of the USSR's GNP (Elnashai, 2002).

The 'business interruption' element of earthquake impact has emerged lately as a major concern to industry and hence to communities. This is the effect of largely non-structural building damage (e.g. suspended light fixtures, interior partitions and exterior cladding) which affects businesses adversely, in turn leading to financial disruption and hardship (Miranda and Aslani, 2003). In several countries, such as the Mediterranean regions and Central America, where tourism is a vital industry, major economic losses have resulted from damage to hotels and negative publicity due to earthquakes. Another aspect of the economic impact is the 'loss of market share' which results from interruption to production in industrial facilities and difficulties in reclaiming the share of the market that the affected business previously held.

The consequences of direct financial losses, business interruption and loss of market share on communities and industry have led major multinationals to create risk management departments in an attempt not only to reduce their exposure, but also to minimise insurance premiums. Global seismic risk management is therefore one of the highest growth areas in industry.

References

Abrahamson, N.A. (1991). Spatial coherency of ground motion from the SMART-1 array. *Geotechnical News*, **9**(1), 31–34.

AIJ (1995). *Performance of Steel Buildings During the 1995 Hyogoken-Nanbu Earthquake*. Architectural Institute of Japan, Tokyo.

Ambraseys, N.N. (1959). A Note on the response of an elastic overburden of varying rigidity to an arbitrary ground motion. *Bulletin of the Seismological Society of America*, **49**(3), 211–220.

Ambraseys, N.N. (1985). Intensity-attenuation and magnitude-intensity relationships for northwest European earthquakes. *Earthquake Engineering and Structural Dynamics*, **13**(6), 733–778.

Ambraseys, N.N. (1989). *Long-Term Seismic Hazard in the Eastern Mediterranean Region, Geohazards, Natural and Man-Made*, Chapman & Hall, New York.

Ambraseys, N.N. (2006). Comparison of frequency of occurrence of earthquakes with slip rates from long-term seismicity data: the cases of Gulf of Corinth, Sea of Marmara and Dead Sea Fault Zone, *Geophysical Journal International* **165**(2), 516–526

Ambraseys, N.N. and Finkel, C. (1986) Corpus of Isoseismal Maps of Eastern Mediterranean Region. Engineering Seismology and Earthquake Engineering. Research Report No. ESEE 86/8, Imperial College, London.

Ambraseys, N.N. and Melville, C.P. (1982). *A History of Persian Earthquakes*. Cambridge University Press, Cambridge.

Ambrose, J. and Vergun, D. (1999). *Design for Earthquakes*. John Wiley & Sons, Inc., New York.

Andreason, K. and Rose, J.D. (1994) Northridge, California Earthquake: Structural Performance of Buildings in San Fernando Valley, California (January 17, 1994). APA Report No. T94-5, American Plywood Association, Tacoma, WA.

Applied Technology Council (1998) Design, Retrofit and Performance of Nonstructural Components. Proceedings of the ATC Seminar, Report No.2-1, Applied Technology Council, Redwood City, CA.

Baker, W.A., Brown, D.H., and Tissel, J.R. (1989) Loma Prieta earthquake, San Francisco Bay Area, October 17, 1989. APA Report No. T89-28, American Plywood Association, Tacoma, WA.

Benioff, H. (1955). Mechanism and strain characteristics of the White Wolf fault as indicated by the aftershock sequence. In *Earthquake in Kern County, California During 1955*, Bulletin No. 171CA (ed. Oakeshott, G.B.), California Division of Mines, pp. 199-202.

Ben-Menachem, A. (1961). Radiation patterns of seismic surface waves from finite moving sources. *Bulletin of the Seismological Society of America*, **51**(2), 401–435.

Bertero, V.V. (2000) Introduction to Earthquake Engineering, http://nisee.berkeley.edu/ebooks/ (accessed 05 January 2015).

Bolt, B.A. (1999). *Earthquakes*. 4th edn, W.H. Freeman and Company, New York.

Bonilla, M.G., Mark, R.K. and Lienkaemper, J.J. (1984). Statistical relations among earthquake magnitude, surface rupture length, and surface fault displacement. *Bulletin of the Seismological Society of America*, **76**(6), 2379–2411.

Broderick, B.M., Elnashai, A.S., Ambraseys, N.N. *et al*. (1994) The Northridge (California) Earthquake of 17 January 1994: Observations, Strong Motion and Correlative Response Analysis. Research Report No. ESEE 94/4, Engineering Seismology and Earthquake Engineering, Imperial College, London.

Bukowski, W. and Scawthorn, C. (1995) Kobe reconnaissance report. Fire. *Earthquake Spectra, Supplement A*, **11**(S1), 33–40.

Clough, R.W. and Penzien, J. (1993). *Dynamics of Structures*. 2nd edn McGraw-Hill, New York.

Coburn, A. and Spence, R. (2002). *Earthquake Protection*. 2nd edn, John Wiley & Sons, Ltd, Chichester.

Der Kiureghian, A. (1996). A coherency model for spatially varying ground motions. *Earthquake Engineering and Structural Dynamics*, **25**(1), 99–111.

Dewey, J.F. (1972). Plate tectonics. *Scientific American*, **226**(5), 56–68.

Durrani, A.J., Elnashai, A.S., Hashah, Y.M.A. *et al*. (2005) The Kashmir Earthquake of October 8, 2005. A Quick Look Report. MAE Center Report No.05-04, University of Illinois at Urbana, Champaign

Elnashai, A.S. (2002). A very brief history of earthquake engineering with emphasis on developments in and from the British Isles. *Chaos Solitons & Fractals*, **13**(5), 967–972.

Elnashai, A.S., Bommer, J.J., Baron, I. *et al*. (1995) Selected Engineering Seismology and Structural Engineering Studies of the Hyogo-ken Nanbu (Kobe, Japan) Earthquake of 17 January 1995. Report No. ESEE/95-2, Engineering Seismology and Earthquake Engineering, Imperial College, London.

Elnashai, A.S., Bommer, J.J. and Martinez-Pereira, A. (1998) Engineering implications of strong motion records from recent earthquakes. Proceedings of the 11th European Conference on Earthquake Engineering, Paris, France.

Federal Emergency Management Agency (2001) HAZUS 1999 Estimated Annualized Earthquake Losses for United States. Report No. FEMA 366, Federal Emergency Management Agency, Washington, DC.

Finn, W.D.L. (1991) Geotechnical engineering aspects of microzonation. Proceedings of the 4th International Conference on Seismic Zonation, Stanford, CA, pp. 199–259.

Goltz, J.D. (1994) The Northridge, California Earthquake of January 17, 1994: General Reconnaissance Report. Report No. NCEER-94-0005, National Centre for Earthquake Engineering Research, Buffalo.

Gutenberg, B. and Richter, C.F. (1936). On seismic waves (third paper). *Gerlands Beitrage zur Geophysik*, **47**, 73–131.

Gutenberg, B. and Richter, C.F. (1956a). Earthquake magnitude. Intensity, energy and acceleration. *Bulletin of the Seismological Society of America*, **46**(1), 105–145.

Gutenberg, B. and Richter, C.F. (1956b). Magnitude and energy of earthquakes. *Annali di Geofisica*, **9**(1).

Haricharan, R.S. and Vanmarcke, E.H. (1986). Stochastic variation of earthquake ground motion in space and time. *Journal of Engineering Mechanics, ASCE*, **112**(2), 154–174.

Housner, G.W. (1965) Intensity of earthquake ground shaking near the causative fault. Proceedings of the 3rd World Conference on Earthquake Engineering, Wellington, New Zealand, Vol. 1, pp. 95–115.

Housner, G.W. (1973) Important features of earthquake ground motions. Proceedings of the 5th World Conference on Earthquake Engineering, Rome, Italy, Vol. 1, pp. CLIX-CLXVIII.

Kanai, K. (1983). *Engineering Seismology*. University of Tokyo Press, Tokyo.

Kanamori, H. (1977) The energy release in great earthquakes. *Journal of Geophysical Research*, **82**(20), 2981–2987.

Kasahara, K.(1981). *Earthquake Mechanics*, Cambridge University Press.

Kramer, S.L. (1996). *Geotechnical Earthquake Engineering*. Prentice Hall, Upper Saddle River, NJ.

Krinitzsky, E. (1974) Fault assessment in earthquake engineering. Miscellaneous Paper S-73-1, Army Engineering Waterways Experiment Station, Vicksburg, MS.

Lee, W.H. K., Kanamori, H., Jennings, P.C. and Kisslinger, C. (2003). *International Handbook of Earthquake and Engineering Seismology*. Academic Press.

Luco, J.E. and Wong, H.L. (1986). Response of a rigid foundation to a spatially random ground motion. *Earthquake Engineering and Structural Dynamics*, **14** (6), 891–908.

Mallet, R. (1862). *Great Neapolitan Earthquake of 1857. The First Principles of Observational Seismology*, vol. 1, Chapman & Hall, London.

Manolis, G.D. and Koliopoulos, P.K. (2001). *Stochastic Structural Dynamics in Earthquake Engineering,* Advances in Earthquake Engineering Series, WIT Press, Southampton.

Mark, R.K. and Bonilla, M.G. (1977) Regression Analysis of Earthquake Magnitude and Surface Fault Length Using the 1970 Data of Bonilla and Buchanan. USGS Open File Report 77–164, U.S. Geological Survey, Menlo Park, CA.

Miranda, E. and Aslani, H. (2003) Building-Specific Loss Estimation Methodology. PEER Report No.2003-03, Pacific Earthquake Engineering Research Center, University of California at Berkeley, Berkeley, CA.

Nuttli, O.W. (1983). Average seismic source-parameter relations for mid-plate earthquakes. *Bulletin of the Seismological Society of America*, **73**(2), 519–535.

Okamoto, S. (1984). *Introduction to Earthquake Engineering*. 2nd edn. University of Tokyo Press, Japan.

Oliveira, C.S., Hao, H. and Penzien, J. (1991). Ground modelling for multiple input structural analysis. *Structural Safety*, **10**(1-3), 79–93.

Osteraas, J. and Krawinkler, H. (1990). The Mexico earthquake of September 19, 1985 – Behavior of steel buildings. *Earthquake Spectra*, **5**(1), 51–88.

Plafker, G. and Galloway, J.P. (1989) Lessons learned from the Loma Prieta California, Earthquake of October 17, 1989. USGS Circular 1045.

Purcaru, G. and Berckhemer, H. (1978). A magnitude scale for very long earthquakes. *Tectonophisics*, **49**, 189–198.

Reiter, L. (1990). *Earthquake Hazard Analysis: Issues and Insights*. Columbia University Press, New York.

Richter, C.F. (1936) An instrumental earthquake magnitude scale. *Bulletin of the Seismological Society of America*, **25**, 1–32.

Richter, C.F. (1958). *Elementary Seismology*. W.H. Freeman and Company, San Francisco, CA.

Sano, T. and Pugliese, A. (1999) Parametric study on topographic effects in seismic soil amplification. *Proceedings of 'Advances in Earthquake Engineering', Earthquake Resistant Engineering Structures II*, G. Oliveto and C.A. Brebbia (Eds), WIT Press, Southampton, Vol. 4, pp. 321–330.

Scawthorn, C., Eidinger, J.M. and Schiff, A.J. (2005) *Fire Following Engineering*. Technical Council on Lifeline Earthquake Engineering, Monograph No. 26, ASCE/NFPA, Reston, VA.

Scholz, C. H. (1990). *The Mechanics of Earthquakes and Faulting*. Cambridge University Press, Cambridge.

Scholz, C.H., Aviles, C. and Wesnousky, S. (1986). Scaling differences between large intraplate and interpolate earthquakes. *Bulletin of the Seismological Society of America*, **76**(1), 65–70.

Seed, H.B., Idriss, I.M. and Kiefer, F.S. (1969). Characteristics of rock motions during earthquakes. *Journal of the Soil Mechanics and Foundations Division, ASCE*, **95**(SM5), 1199–1218.

Silva, W.J. (1988) Soil Response to Earthquake Ground Motion. Report No. EPRI-NP-5747, Electric Power Research Institute, Palo Alto, CA.

Singh, J.P. (1985). Earthquake ground motions: implications for designing structures and reconciling structural damage. *Earthquake Spectra*, **1**(2), 239–270.

Slemmons, D.B. (1977) State-of-the-Art for Assessing Earthquake Hazards in the United States: Report 6, Faults and Earthquake Magnitude. Miscellaneous Paper S-173-1, US Army Corps of Engineers, Waterways Experiment Station, Vicksburg, MS.

Somerville, P., McLaren, J.P., Mrinal, K.S. and Helmberg, D.V. (1991). The influence of site conditions on the spatial incoherence of ground motions. *Structural Safety*, **10**(1–3), 1–13.

Somerville, P.G., Smith, N.F., Graves, R.W. and Abrahamson N.A. (1997). Modification of empirical strong motion attenuation relations to include the amplitude and duration effects of rupture directivity. *Seismological Research Letters*, **68**(1), 199–222.

Sponheuer, W. (1960). *Methoden zur Herdtiefenbestimung in der Madkroseismik*. Akademic Verlag, East Berlin.

Steinbrugge, K.V. (1982). *Earthquakes, Volcanoes and Tsunamis: An Anatomy of Hazards*. Skandia America Group, New York.

Stewart, J.P., Chiou, S.J., Bray, J.O. *et al*. (2001) *Ground Motion Evaluation Procedures for Performance-Based Design*. Report No. PEER 2001/9, Pacific Earthquake Engineering Center, University of California, Berkeley, CA.

Street, R.L. and Turcotte, F.T. (1977). A study of northeastern North America spectral moments, magnitudes and intensities. *Bulletin of the Seismological Society of America*, **67**(3), 599–614.

Taylor, C., Mittler, E. and LeVal, L. (1998) *Overcoming Barriers: Lifeline Seismic Improvement Programs*. Monograph No. 13, Technical Council on Lifeline Earthquake Engineering, ASCE, Reston, VA.

Taylor, C. and VanMarcke, E. (2002) *Acceptable Risk Processes: Lifelines and Natural Hazards*. Monograph No. 21, Technical Council on Lifeline Earthquake Engineering, ASCE, Reston, VA.

Tocher, D. (1958). Earthquake energy and ground breakage. *Bulletin of the Seismological Society of America*, **48** (1), 147–153.

Udias, A. (1999). *Principles of Seismology*. Cambridge University Press, Cambridge.

Wells, D. L. and Coppersmith, K.J. (1994). New empirical relationships among magnitude, rupture length, rupture width, rupture area, and surface displacement. *Bulletin of the Seismological Society of America*, **84**(4), 974–1002.

Wyss, M. (1979). Estimating maximum expectable magnitude of earthquakes from fault dimensions. *Geology*, **7**(7), 336–340.